ANNALS OF GEOPHYSICS, 65, 5, S552, 2024; doi:10.4401/ag-9137
OPEN ACCESS

MASLIS: A five-year review of Costa Rica's near real-time seismic intensity processing system

Aaron Moya[*,1]

[(1)] Laboratorio de Ingeniería Sísmica, Universidad de Costa Rica

Article history: received August 7, 2024; accepted November 6, 2024

Abstract

The MASLIS is an online system that displays the earthquake's seismic intensity in near-real time. The system analyzes the data from Costa Rica's strong motion network. When the intensity exceeds a specified intensity threshold at a number of sites, the system sends several warning messages. When it was first developed in 2019, the system was tested using scenario earthquakes. After five years of operation, this article briefly discusses its performance using actual earthquake data.

Keywords: Costa Rica; Strong motion; Earthquake early warning; Acceleration; JMA intensity

1. Introduction

In its simplest form, an earthquake early warning system (EEWS) delivers messages about an impending, damaging earthquake, before the strong seismic waves arrive to a specific place. They all take advantage of the fact that the compressional waves (P-waves) travel faster than the damaging shear waves (S-waves). The P-waves must first trigger one or several recording sensors and data has to be analyzed on-site or by a remote server in order to decide where warnings should be issued. There are many different ways in which an EEWS can be implemented (Allen and Melgar, 2019), but in general, they can be classified into two large groups: regional and on-site. The first one uses a dense network of instruments in order to calculate the source parameters to later predict the the ground motion at sites of interest. The second one, on the contrary, uses a single instrument to predict the ground motion using the first seconds from the P-wave arrival. Both have advantages and disadvantages.

In Mexico, the EEWS (SASMEX) (Espinosa-Aranda et al., 1995) consists of more than 90 stations, most of them located along the subduction zone. Each monitoring station analyzes the seismic waves independently and calculates some strong motion parameters that are correlated empirically to a moment magnitude threshold. When the established threshold is surpassed by two nearby stations, the information is sent to a central facility which decides where to emit an alert (Suárez, 2022). In this specific case, the precise location and magnitude of the earthquake are not critical. Also, the information delivered to the public omits the strength of ground shaking or the warning time before the S-waves arrive.

In the Western United States the ShakeAlert system (Burkett et al., 2014) and in Japan the JMA EEW (Hoshiba et al., 2008), on the other hand, must first try to determine the earthquake source parameters as accurately as possible. They are needed in order to predict the ground motion at specific sites where the warning messages will be delivered. Unfortunately the recent 2019 Ridgecrest and 2011 Tohoku earthquakes respectively, underestimated the real

magnitude thus failing to communicate the pricise shaking intensity to the recipients (Chung et al., 2020; Fujinawa and Noda, 2013; Hoshiba and Iwakiri, 2011). However, after those experiences, the algorithms were improved in order to overcome similar difficulties from potential future events (Lux et al., 2024; Kodera et al., 2021).

Taiwan has three EEWS (Wu et al., 2021). The regional one is operated by the Central Weather Bureau (CWB) and can provide alarms to the public about 17 s after earthquake's occurrence. The system has not experienced any false alarm since it started operations. The second one is called P-Alert, and it is an on-site as well as regional EEWS. This one consists of Micro-Electronic-Mechanical Systems (MEMS) instruments that are mainly located in elementary schools. Finally, the third EEWS is called NEEWS acts as an on-site system and predicts peak ground acceleration values based on the first seconds of the detected P-waves.

The Chinese EEWS started as a major pilot program deployed in several provinces. In Fujian province the monitoring stations contain both an accelerometer and velocimeter instruments and in 2017 the system started issuing public alerts (Zhang et al., 2021). In Sichuan province there are over 2000 units spaced an average distance of 12 km (Peng et al., 2021) where a Java based EEWS processes the information. Italy uses the PRobabilistic and Evolutionary early warning SysTem (PRESTo) which is a free and open source platform (Satriano et al., 2011). In Turkey a series of strong motion sensors were deployed along the Marmara Sea region where a strong earthquake is expected to occur. This EEWS will not estimate the source parameters of the earthquake but rather will send notification that a strong shaking is taking place in the area (Clinton et al., 2016).

In Costa Rica, Protti (2001) proposed the implementation of an EEWS to warn of earthquakes, especially on the Pacific coast. Porras et al. (2021) evaluated the performance of an EEWS using the network from the Red Sismológica Nacional (RSN), while the Observatorio Vulcanológico y Sismológico de Costa Rica (OVSICORI) implemented another one that included the use of fixed smartphones (Brooks et al., 2021). This article outlines the progress of the Monitoreo Acelerográfico Secundario del Laboratorio de Ingeniería Sísmica (MASLIS) since it became public in 2019 (Moya, 2019). The MASLIS was not initially intended to be used as an EEWS, but it could evolve into one because of its rapid assessment of seismic intensity.

The MASLIS looks for variations in seismic intensity to identify the occurrence of an earthquake, rather than the usual approach of first identifying the P-waves. Once activated, the system sends a warning message indicating the occurrence of an earthquake anywhere in the country. At present, the MASLIS does not aim to predict ground motion or identify target areas for issuing alerts.

2. Tectonic setting

There are two main sources of seismicity in Costa Rica. One is the subduction of the Cocos plate under the Caribbean plate, and the other is local faulting. The Cocos plate subducts under the Caribbean plate along the Middle America Trench (Fig. 1), and it is responsible for most of the events that take place along the Pacific coast. The earthquakes shown in Fig. 1 correspond to those recorded by the strong motion network that the Laboratorio de Ingeniería Sísmica from the University of Costa Rica (LISUCR) operates. The magnitude ranges from 2 to 7.6. There are two main clusters: one in the middle of the country and the other close to the Panama border. The region in between has a low seismicity rate influenced by the geometry of the subducting plate and the presence of the Cocos Ridge (Lücke and Arroyo, 2015). The Cocos plate subducts with a steeper angle in the northern part (Husen et al., 2003), which explains the deep-focus earthquakes that can be seen in the north-south and east-west profiles in Fig. 1. In southern Costa Rica, the Panama Fracture Zone (PFZ) marks the limit between the Cocos Plate and the Nazca plate along a series of right-lateral transform faults (Morell et al., 2008).

Subduction zone earthquakes can reach magnitudes above 7 (Bird, 2003; Ye et al., 2013), although recent ones have occurred far from the capital (Fig. 2). Because of this, the peak ground acceleration (PGA) values recorded in San Jose have been relatively low. For instance, the March 25th, 1990, M7.0 (Protti et al., 1995), the August 20th, 1999, M6.9 (Bilek and Lithgow-Bertelloni, 2005), and the September 5th, 2012, M7.6 (Yue et al., 2013) earthquakes produced 86, 47, and 83 gals in the capital respectively. In terms of intensity, they reached a maximum of 4 on the Japan Meteorological Agency scale (JMA) with no significant damage reported in the capital. Conversely, the November 20th, 2004, M6.2 (Pacheco et al., 2006) earthquake was situated 46 km from San Jose and was a much smaller event in magnitude. The corresponding JMA intensity was also 4; however, the recorded PGA was 180 gals. This suggests that the proximity of the subduction zone, specially in the middle of the country, poses a significant threat to the city.

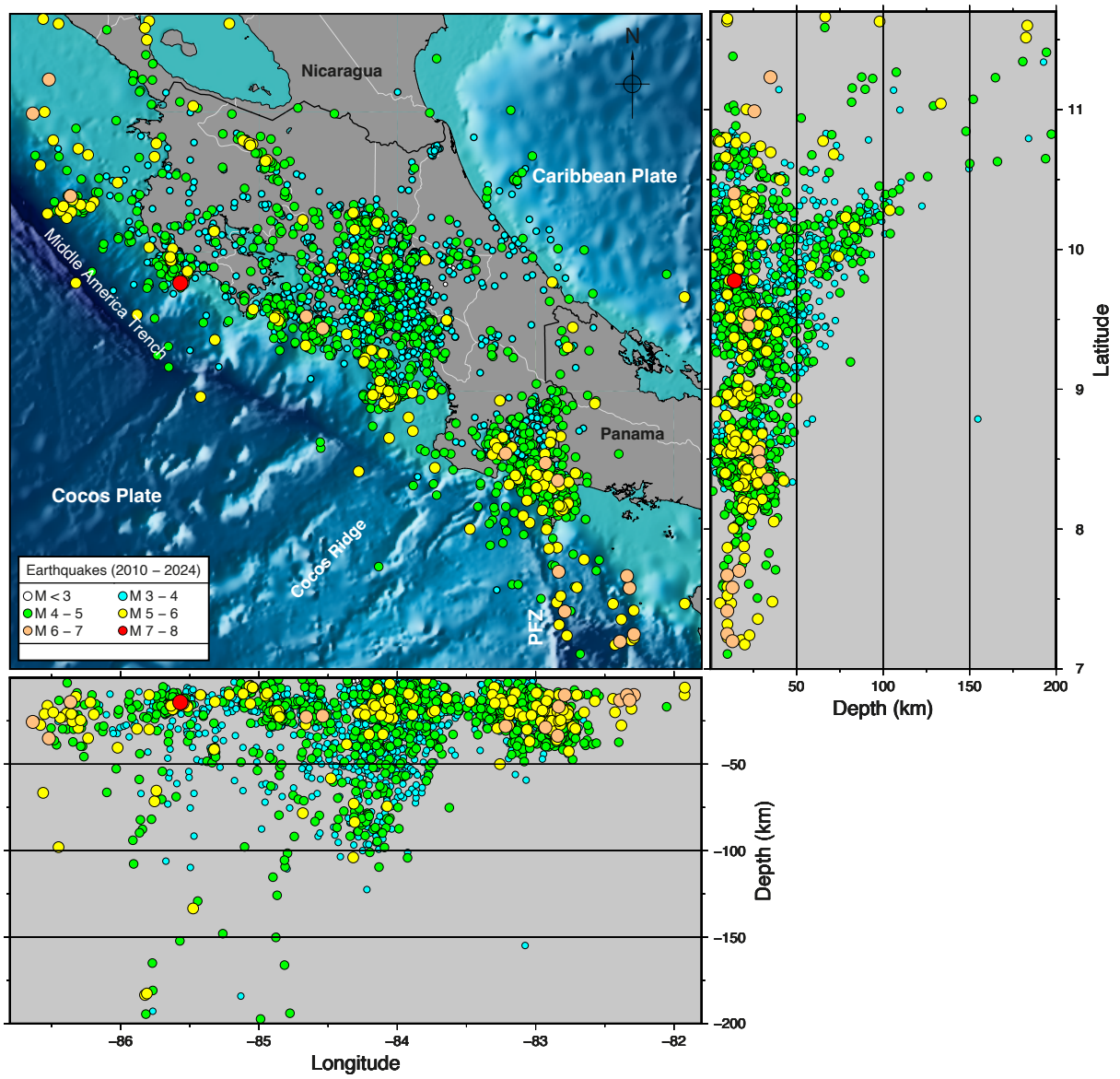

Figure 1. Earthquakes recorded by the LISUCR from 2010 to 2014 and tectonic setting. The Cocos plate subducts under the Caribbean plate along the Middle America Trench. In southern Costa Rica, the Panama Fracture Zone (PFZ) is responsible for much of the seismic activity in that area.

The earliest recorded event by the LISUCR's network took place on April 3rd, 1983, when an Ms7.3 struck southern Costa Rica (Adamek et al., 1987; Tajima and Kikuchi, 1995; Fig. 2). According to the United States Geological Survey (USGS), the epicenter was located northeast of the Golfito city 37 km deep. Much damage was reported in the epicentral area. At that time, the country had only a few strong motion instruments and they were located only in San Jose. The PGA recorded in the capital was 47.1 gal on the university campus. The estimated JMA intensity was 3.

Local faulting earthquakes are a particular concern since they can happen very close to major cities. San Jose, Cartago, Heredia, and Alajuela are part of the Greater Metropolitan Area (GAM in Spanish), where 60% of the population lives. Figure 3 shows the location of major active faults (red lines) in central Costa Rica and some significant earthquakes that damaged structures and caused numerous deaths. The most important one was an Ms6.4 that occurred in 1910 and devastated Cartago with a death toll of over 600 casualties (Alonso-Henar et al., 2013). The number of deaths was exceptionally high considering that, at the beginning of the century, the city's population was around twelve thousand inhabitants. In fact, that single event has been the worst earthquake-related disaster in Costa Rican history. Most of the deaths were due to the collapse of adobe and bahareque houses that could not withstand the shaking. There were no strong motion records from that time. The photographic record of

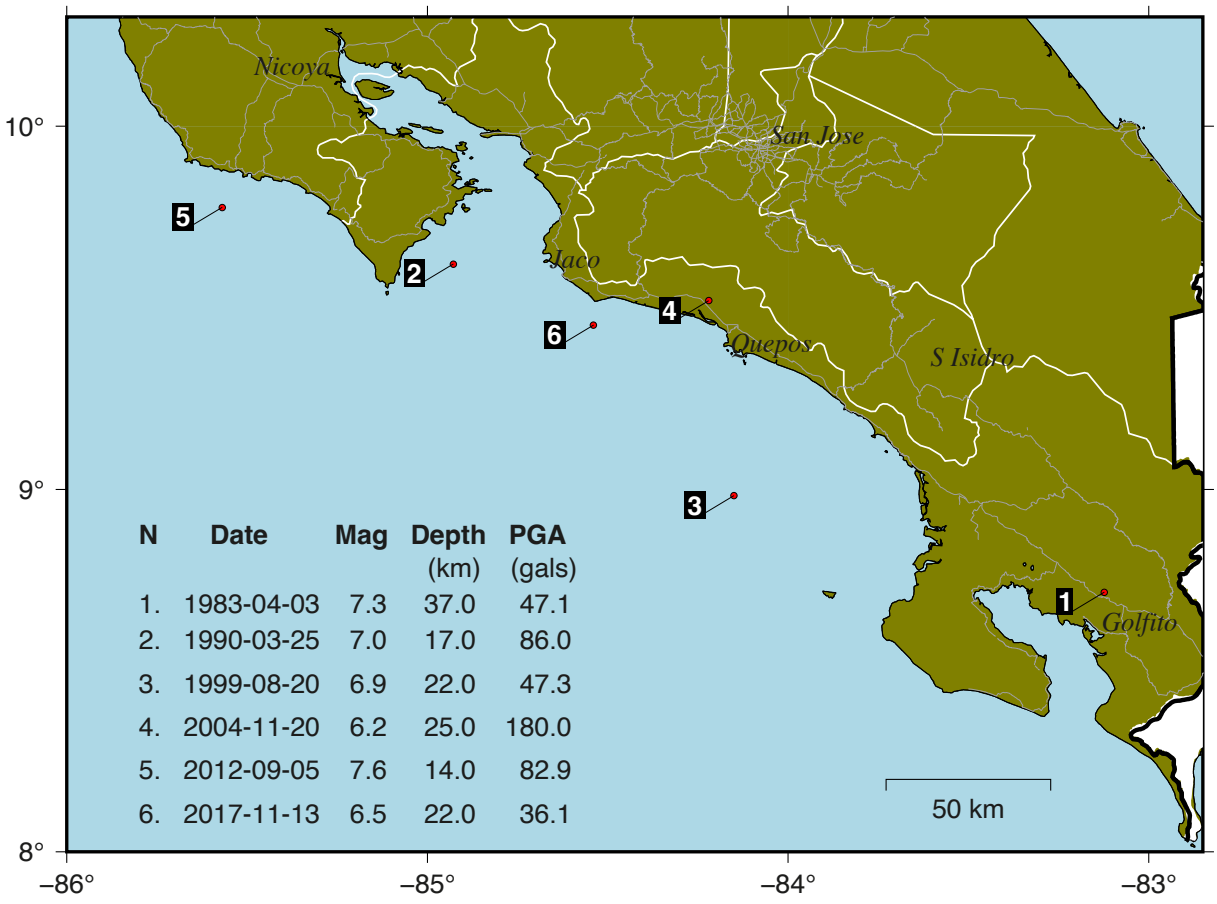

Figure 2. Selected major earthquakes along the Pacific subduction zone from 1983 to 2017. The inserted table shows the date, magnitude, depth in kilometers, and peak ground acceleration in gals recorded in San Jose.

the destruction indicates that the earthquake had to be a shallow event with high acceleration values from the movement of massive stone structures.

In 1990, an M6.0 earthquake struck in the western part of the GAM. In Alajuela city, many houses collapsed or were severely damaged (Bilek et al., 2009). The PGA recorded in central Alajuela was 415 gals and the JMA intensity was 6–. In San Jose, the PGA was 220 gals and JMA = 5+. That remained the largest PGA value recorded for an inland earthquake in Costa Rica before the January 8th, 2009 event occurred.

The 2009 earthquake struck 30 km north of San Jose, and was the most destructive inland event in recent years (Quesada-Román and Barrantes-Castillo, 2016). The PGA recorded close to the epicenter was 658 gals with an intensity JMA = 6–. In the capital city, the acceleration was 175 gals, and the corresponding intensity JMA = 5–. It had a shallow focus located in a volcanic region of difficult access and characterized by steep slopes. For that reason, the earthquake triggered many landslides that destroyed roads and affected several communities and factories. There were more than 20 fatalities.

3. Strong Motion Network

The LISUCR has a strong motion network composed of a total of 179 digital accelerographs. They are located in free-field, buildings, and borehole stations inside protective metal boxes. There are 127 free-field stations. The stations are unevenly distributed throughout the country (Moya-Fernandez et al., 2020), as shown in Fig. 4. Many are placed within the GAM. Another group of stations is located along the Pacific coast, where large magnitude earthquakes are more likely to occur (Hidalgo-Leiva et al., 2022), with fewer stations found in the eastern (Caribbean) and northeastern regions. In spite of the historically low seismic activity in the Caribbean, a powerful M7.7 earthquake caused widespread damage from Costa Rica to Panama in 1991 (Goess et al., 1993; Suárez et al., 1995).

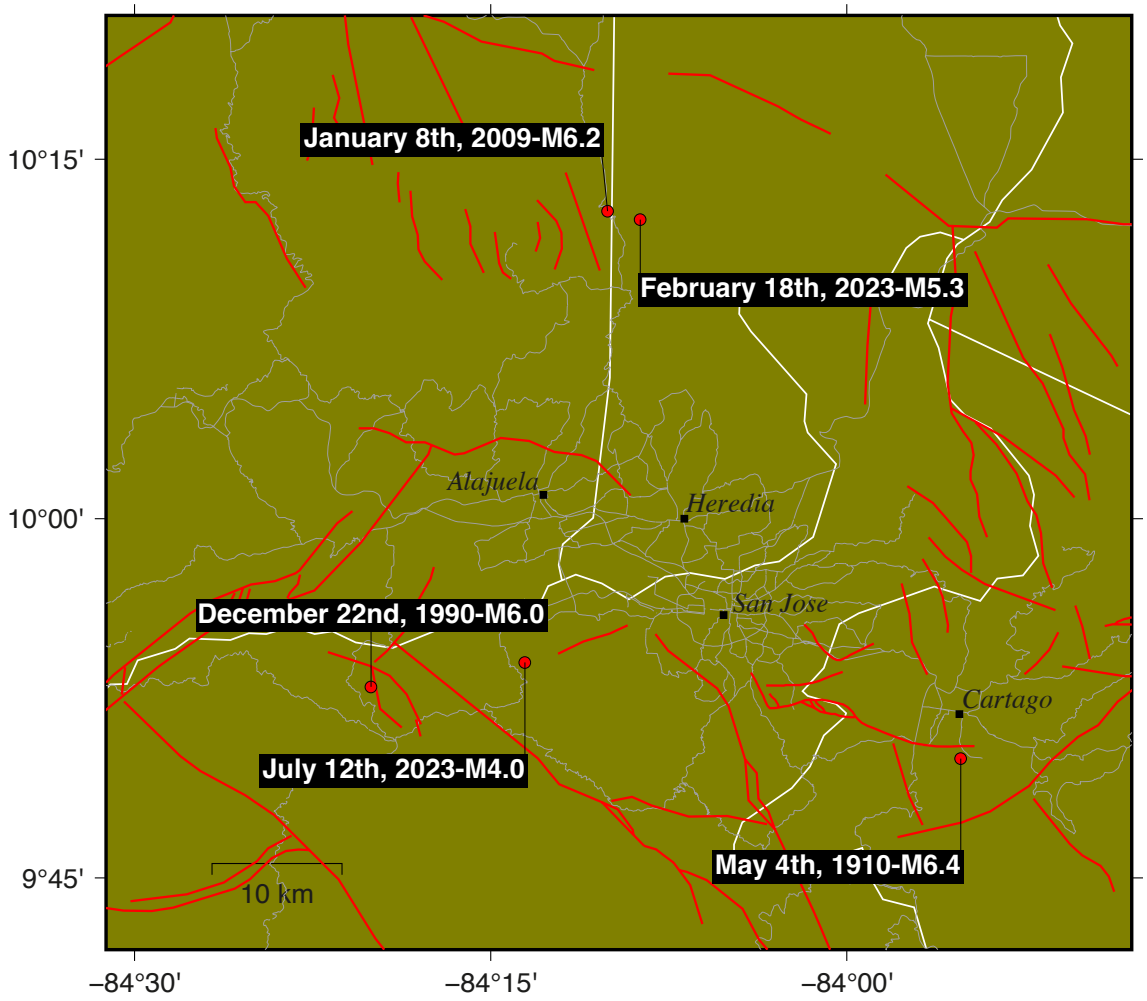

Figure 3. Locations of three of the destructive earthquakes from 1910, 1990, and 2009 around the GAM in Costa Rica. Major urban areas are shown by dark squares. Gray lines correspond to main roads. White lines correspond to administrative divisions (provinces). Red lines show Quaternary active faults. The events on February 18th and July 12th, 2023, were recorded by the MASLIS.

In 2010, the Sistema de Monitoreo Acelerográfico del Laboratoio de Ingeniería Sísmica (SMALIS) (Moya, 2017) was developed in order to automatically process the information coming from all instruments. The system calculated the earthquake's source parameters as well as the seismic intensity, design and response spectra, duration, building and borehole spectral ratios, etc. Information was posted on the Internet at https://www.lis.ucr.ac.cr, and it was also sent out to the public through social networks such as X, Telegram, and e-mail previously.

As the network grew larger with the addition of new stations (such as 12 in collaboration with the OVSICORI and several new buildings), the processing of all information became a very time-consuming task that took no less than 30 minutes to be completely finished. During large earthquakes, especially, it was crucial to identify the most affected areas as soon as possible.

The MASLIS was released in 2019 as a fast alternative to the SMALIS. The purpose was to inform on seismic intensity, PGA, and preliminary source parameters in near real-time. When an earthquake occurred, the system delivered a series of warning messages indicating that such an event had been detected by displaying the seismic intensity of stations. Unlike the SMALIS which processes information from all stations, the MASLIS uses only the free-field stations.

The original version was designed to carry out all calculations every 5 seconds. In 2022, the code was revised resulting in an average time interval of 2-3 seconds. Due to its speed, when an earthquake was detected (depending on its location), the warning messages sometimes reached the public before they could actually feel the ground shaking. People began to consider the MASLIS as a potential EEWS, although it did not completely fit that description.

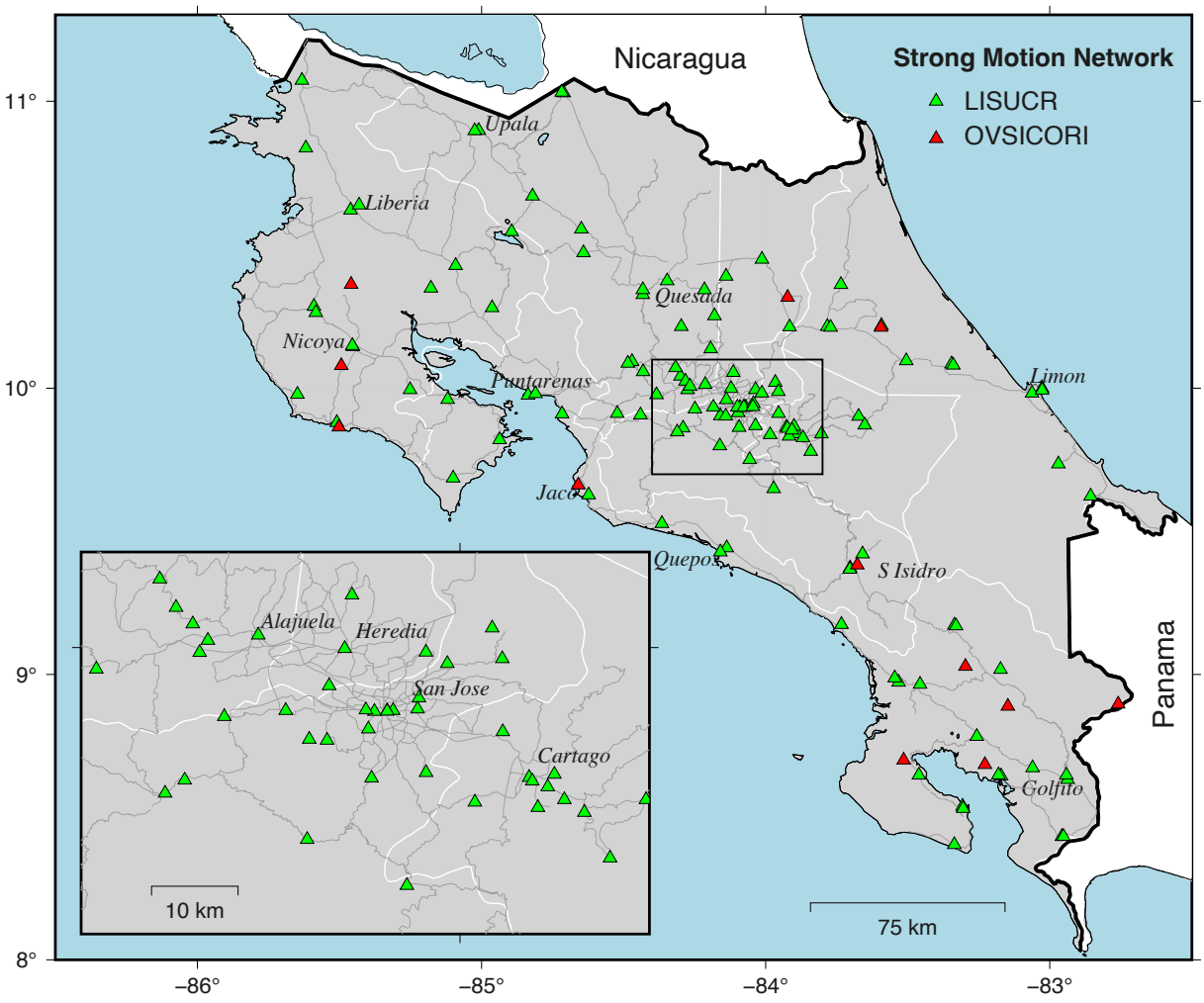

Figure 4. The MASLIS processes information from 127 strong-motion stations from LISUCR (green triangles) and 12 from OVSICORI (red triangles). Gray lines correspond to major roads, while white lines indicate administrative divisions.

The purpose of the MASLIS is to quickly notify where the shaking is strongest as soon as an earthquake is detected. This is achieved by calculating the JMA intensity scale described in Shabestari and Yamazaki (2001) at each time interval. The JMA intensity has the advantage that no prior information about the earthquake's source parameters is needed.

4. How the MASLIS works

The MASLIS scans the strong-motion network (Fig. 5) every 2-3 seconds on average. It reads a 2-minute time window from every station. The system checks for any data gaps in the three-component record and computes the JMA intensity scale. At each time-step, a table is generated that contains the name of the station, its location, PGA, and JMA intensity values.

Two criteria have to be met before the system activates. The first one is that the intensity at a given number of sites has to be larger than a specified threshold, which is JMA = 1. The second one is that at least three of the sites should be located within a 0.5-degree distance. This ensures that the stations that exceed the JMA = 1 threshold are related to the same event, ruling out random triggers like sensor malfunctions.

The MASLIS issues a total of five warning messages when an earthquake is detected. The message consists of a map, as depicted by Fig. 6. The map shows the JMA intensity at the stations. The bottom left corner displays the names of the five sites where the highest intensity was recorded. The intensity values are presented in brackets and are organized in descending order, while the PGA values are shown in parentheses in gals.

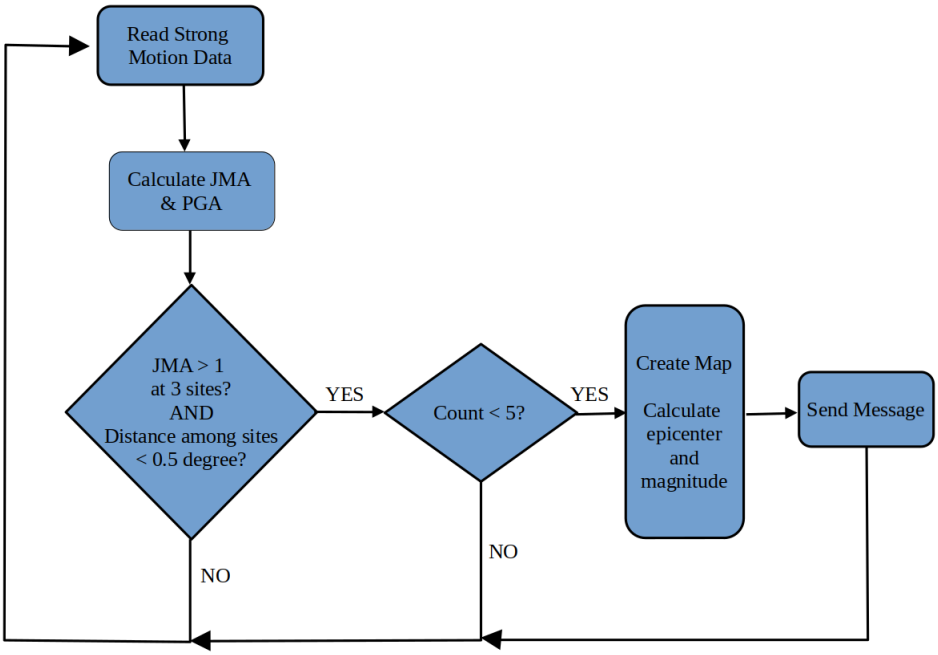

Figure 5. Diagram showing the MASLIS processing system. The strong motion data is read and processed to calculate the JMA intensity and PGA. If JMA exceeds 1 in three locations, the system gets triggered. It then generates a map and issues an alert indicating the detection of an earthquake. This process is repeated five times.

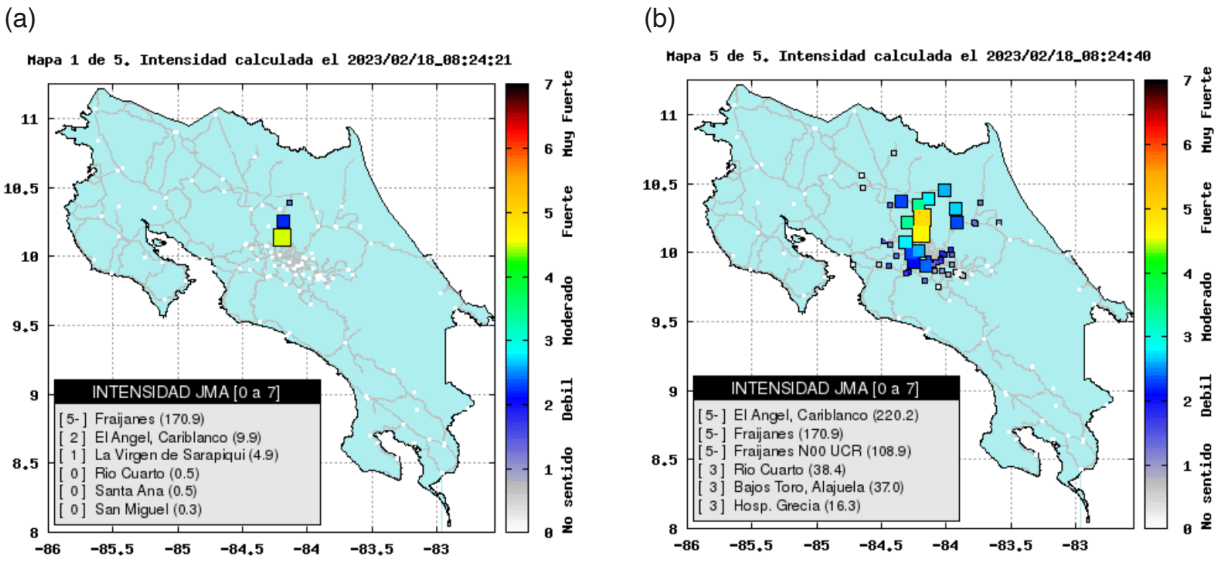

Figure 6. Examples of warning messages provided by the MASLIS. This corresponds to the February 8th, 2023, M5.3 earthquake located north of San Jose. (a) Shows the initial map when the system was activated. (b) Shows the fifth map. The table in the lower left corner displays the JMA intensity in square brackets, the station name, and the PGA in gals in parentheses. The first five sites with the highest intensity values are listed in descending order. The right side shows the JMA intensity scale.

When the system is triggered, MASLIS also tries to calculate the source parameters. The waveform data is processed by an automatic phase picking algorithm in SAC (Goldstein and Snoke, 2005) to determine the P-wave arrival times from all available stations. Then, the non-linear earthquake location program (NLLoc) from Lomax et al. (2000) is used to calculate the epicenter.

The magnitude is estimated using the following procedure. First, the acceleration spectra from each station is converted to displacement and corrected by geometrical spreading. The low-frequency flat level, Ω_0, is read from

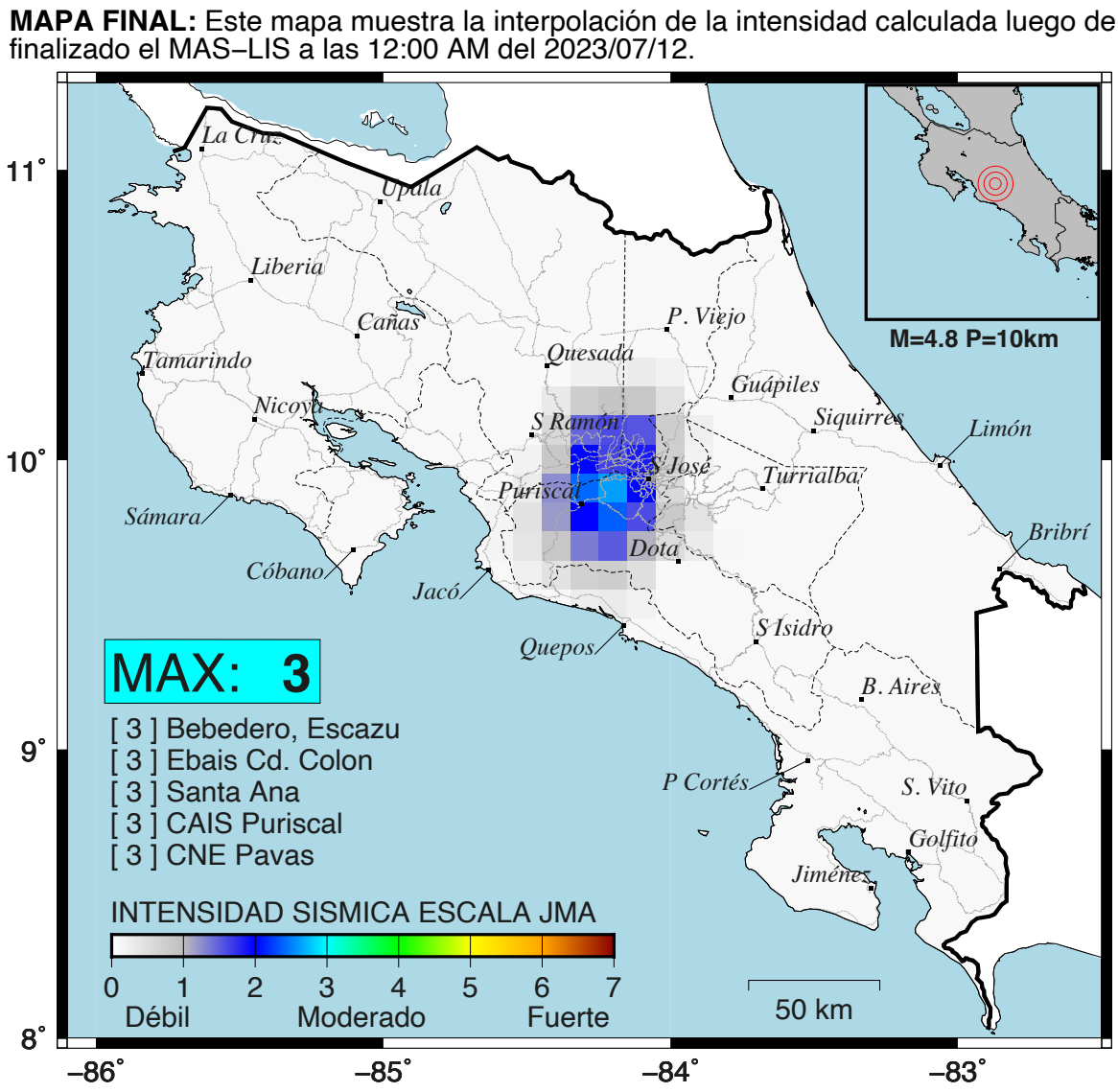

Figure 7. The sixth and final map generated by the MASLIS. This plot is produced after the earthquake has finished. This result corresponds to a small event located in the middle of the country with a preliminary magnitude of 4.8 at a depth of 10 km shown in the upper right corner. The map shows the interpolated seismic intensity values. The overall maximum is displayed in a colored box that changes according to the JMA scale, in this case 3. A brief description of the expected damage for the largest JMA value is shown at the bottom of the image. Gray lines correspond to major roads, dotted lines correspond to provinces.

the vectorial summation of the horizontal components. The seismic moment, Mo, is then calculated assuming a Brune's (1970) source model:

$$Mo = 4\pi\rho\beta^3\,\Omega_0/R_{\phi\theta} \tag{1}$$

where ρ is the density 2.7 g/cm^3, β is the S-wave velocity 3.2 km/s, and $R_{\phi\theta}$ is the radiation pattern taken as $\sqrt{(2/5)}$ (Andrews, 1986). Finally, the moment magnitude, Mw, is obtained from Hanks and Kanamori (1979) using the following equation:

$$Mw = \frac{2}{3}\log_{10}Mo - 10.7 \tag{2}$$

The JMA intensity and source parameters are updated each time new waveform data arrives. Usually, the most heavily impacted areas can be identified by the time the second message is delivered. This allows emergency attention to be prioritized before the epicenter's precise location or magnitude's final estimation is determined.

When there is a moderate to large magnitude earthquake, the seismic waves may not reach the distant stations by the time the fifth message gets delivered. This happens because big events have a duration that exceeds the MASLIS processing time. To create a final map displaying the overall intensity, the system generates a sixth map after the shaking has ended. The final map shows the interpolated intensity from the highest values recorded by each station (Fig. 7). Interpolation is done with the *surface* algorithm from the GMT package (Wessel et al., 2013) using a 0.1-degree mesh.

5. MASLIS performance

When the MASLIS was first released in 2019, the trigger threshold was set to JMA = 2 at two sites. That was sufficient when the epicenter was close to the stations, and the seismic waves were rather impulsive. The JMA = 2 criterion was quickly reached under those circumstances, generally for moderate-magnitude earthquakes. However, the case was different for large-magnitude and distant events (particularly those from offshore Nicaragua and the PFZ; see Fig. 8). Costa Rican borders are a region of sparse station coverage. Also, the incoming seismic waves were

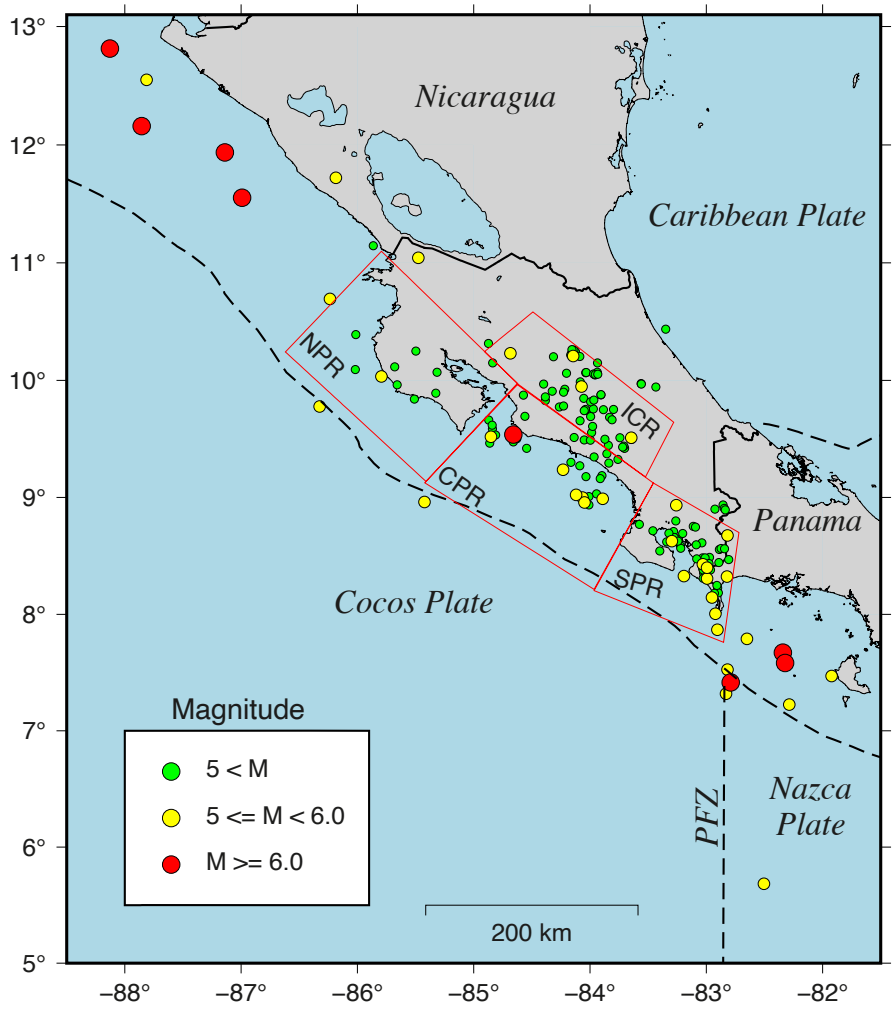

Figure 8. Earthquakes recorded by the MASLIS from September 2019 until May 2024. The events are shown by magnitude. The plate borders are shown as dotted lines. The red polygons correspond to the seismogenic zones mentioned in the text: NPR: Northern Pacific Region, CPR: Central Pacific Region, SPR: Southern Pacific Region, and ICR: Inland Central Region. PFZ: Panama Fracture Zone.

emergent ones. The latter means that the initial waveform is very small, thus delaying the time needed to reach the JMA = 2 threshold. This fact also affects EEWSs that depend on rapid estimation of source parameters. During the 2011 Japan earthquake, M9.1, the initial magnitude was estimated at 4.3 because the first P-waves detected by the closest station were comparable to the noise level for displacement (Hoshiba and Iwakiri, 2011).

Although the MASLIS detected strong offshore events, the activation times were rather late for the reasons already explained. To avoid this, in 2022, the trigger threshold was changed from JMA = 2 at two sites to JMA = 1 at three sites. Following the Ridgecrest events in 2019, the alerting threshold for the ShakeAlert system for the city of Los Angeles was lowered from light to weak shaking. The reason was that people wanted to receive notifications even for non-damaging levels of shaking (Wald, 2020).

This change had an impact on the number of events recorded, as shown in Table 1. Small-magnitude events can easily trigger the MASLIS when they occur close to a recording station. They generally produce high intensity values of PGA and JMA. For example, in the year 2022, the system recorded a total of 36 events with magnitudes ranging from M3.5 to M6.7. The largest PGA was from the M3.5 event occurring on February 24th, 2022 (see Table 1). The epicenter was located just 1 km from the recording station and produced JMA = 3.

Year	Number	Magnitude range	Date (Magnitude) PGA in gals
2019 (from September)	11	4.2-5.1	2019-12-18 (M5.1) 338.3
2020	26	4.1-6.0	2020-03-06 (M5.4) 610.6
2021	25	3.7-6.7	2021-04-10 (M4.8) 132.0
2022	36	3.5-6.7	2022-02-24 (M3.5) 133.6
2023	63	3.3-6.5	2023-02-18 (M5.3) 229.0
2024 (until May)	22	3.6-5.7	2024-05-25 (M5.2) 208.5

Table 1. Number of earthquakes processed by the MASLIS since 2019 by year. The table also shows the minimum and maximum magnitude recorded within each year. The last column shows the earthquake's date (and magnitude) of the corresponding event with the highest PGA value recorded.

Table 2 groups the earthquakes according to the general seismogenic regions depicted in Fig. 8. It also shows the number of events deeper than 50 km. Most of the earthquakes are located in the Inland Central Region (ICR) due to the concentration of recording stations (Fig. 4). Ten earthquakes happened at depths greater than 50 km in the ICR. There are also many events in the SPR mostly related to shallow sources.

The MASLIS performance was evaluated by analyzing the time it took for the system to detect an earthquake, process the information, and then finally deliver a warning message. Eight earthquakes were chosen from four of the seismogenic zones listed in Table 2. They were selected because of their proximity to previous major earthquake epicenters, allowing us to estimate the approximate warning times for potential future events. Their source parameters and distance to San Jose are shown in Table 3.

Table 4 displays the various data processing times for the events listed in Table 3. After the origin time, OT, the seismic waves travel at different speeds. In this article, we will assume that the P-wave velocity is 6 km/s and the S-wave velocity is 3.5 km/s. When the seismic waves reach the surface, they are recorded by different monitoring stations while still propagating (Fig. 9). The activation time, AT, is when the MASLIS detects the earthquake. CT is when the system finishes processing all information, including the warning message and intensity maps. TT is when

Seismogenic Zone	Depth (< 50 km)	Depth (> 50 km)	Total number
Northern Pacific Region (NPR)	9	1	10
Central Pacific (CPR)	33	0	33
Southern Pacific (SPR)	49	1	50
Inland Central Region (ICR)	51	10	61
Eastern Region	3	0	3
Other	22	4	26

Table 2. Total number of earthquakes processed by the MASLIS by seismogenic zone and depth.

N	Origin Time (OT) Y-M-D H:M:S (UTC)	Magnitude (Mw)	Depth (km)	Longitude	Latitude	Distance to San Jose (km)
1	2019-12-08 18:31:42	5.1	29.9	-85.793	10.033	190.4
2	2021-07-21 21:15:12	6.7	10.0	-82.789	07.416	308.4
3	2023-04-04 22:18:12	6.4	13.0	-82.321	07.583	326.0
4	2020-03-07 02:40:45	5.4	50.0	-83.258	08.934	140.0
5	2022-05-08 00:25:38	5.2	14.7	-83.295	08.627	165.6
6	2020-08-24 21:51:08	6.0	22.7	-84.658	09.538	79.2
7	2023-02-18 08:24:12	5.3	6.5	-84.145	10.208	31.6
8	2023-07-12 05:58:41	4.0	2.9	-84.226	09.900	19.3

Table 3. Source parameters of selected earthquakes and epicentral distances to San Jose. The order is determined by how they are presented in the text.

the message is posted on Telegram. Figure 9 visually shows the wave propagation during the AT, CT, and TT stages of data processing in the MASLIS.

The AT-OT time difference varies significantly depending on the earthquake's location and depth. The AT-OT is small for shallow focus and near-to-the-station earthquakes (e.g. events number 7 and 8 in Tables 3 and 4) and significant for deep or distant events. The CT-AT time difference is the total processing time in seconds. This time may vary depending on the number of stations the system has to manage in the initial time step.

N	Origin Time (OT) (Y-M-D H:M:S) (UTC)	AT (H:M:S)	CT (H:M:S)	TT (H:M:S)	AT-OT (s)	CT-AT (s)	TT-CT (s)	TT-OT (s)	SR (km)	RT (s)	NS
1	2019-12-08 18:31:42	18:31:57	18:32:06	18:32:08	15	9	2	26	92	28	4
2	2021-07-21 21:15:12	21:15:45	21:15:56	21:15:58	33	11	2	46	162	41	8
3	2023-04-04 22:18:12	22:18:38	22:18:45	22:18:47	26	7	2	35	132	51	5
4	2020-03-07 02:40:45	02:40:57	02:41:08	02:41:11	12	11	3	26	90	15	7
5	2022-05-08 00:25:38	00:25:47	00:25:53	00:25:54	9	6	1	16	55	32	3
6	2020-08-24 21:51:08	21:51:21	21:51:32	21:51:34	13	11	2	26	84	-1	23
7	2023-02-18 08:24:12	08:24:18	08:24:24	08:24:26	6	6	2	14	45	-1	3
8	2023-07-12 05:58:41	05:58:48	05:59:01	05:59:04	7	13	3	23	66	-1	5

Table 4. Different processing times in the MASLIS for the selected events in Table 3. OT: UTC origin time in the format Year-Month-Day Hour:Minute:Second. AT: This is the time in hour, minute, and second when the MASLIS detects an earthquake. CT: This is the time when the information has been processed (message and maps). TT: This is the time when the information reaches its final destination on the recipient's device. The differences AT-OT (activation time), CT-AT (processing time), TT-CT (posting time), and TT-OT (total time) are the time in seconds in each of the processing steps. SR: Distance in kilometers the S-waves have traveled during the interval TT-OT. RT: Remaining time in seconds ("warning time") before the S-waves arrive in San Jose, a "−1" indicates that there is no warning time. NS: Initial number stations with JMA > 1.

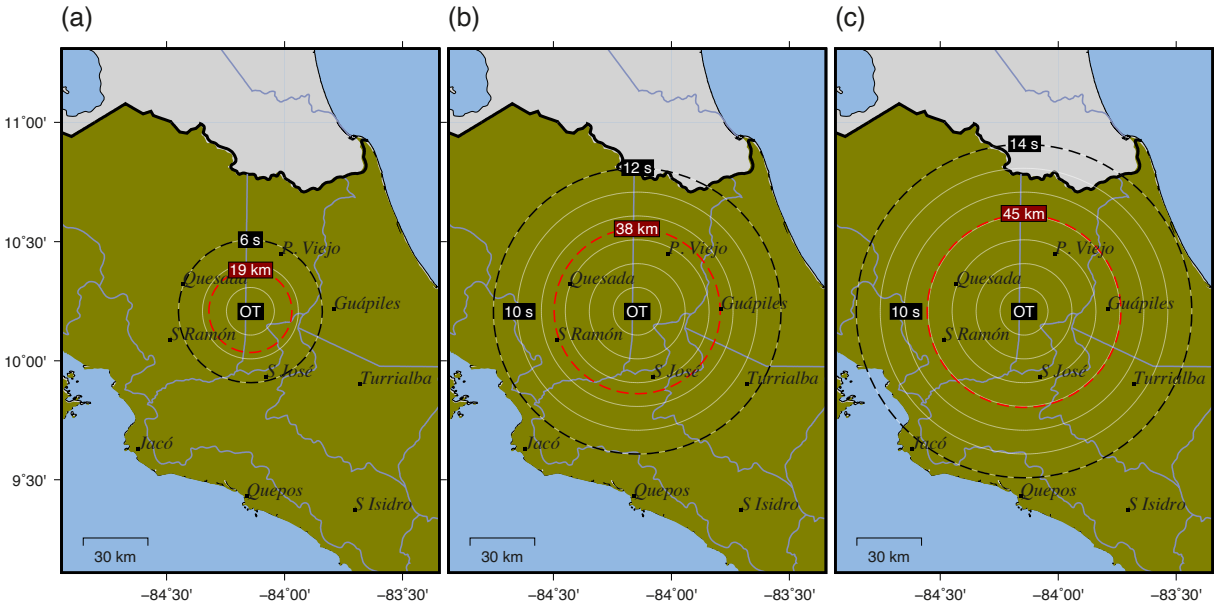

Figure 9. The figure shows the P and S wave propagation fronts during (a) activation time (AT), (b) processing time (CT), and (c) posting time (TT) for event number 7 in Tables 3 and 4. Black dotted circle corresponds to the approximate location of the P-wave front in seconds after OT. Red dotted circle shows the distance traveled by the S-wave from the source. White lines are P-wave propagation times every 2 seconds.

5.1 Northern Pacific Region

On December 8th, 2019, an M5.1 earthquake occurred off the coast of the northern Pacific. The peak intensity was JMA = 5–, recorded at a station located 10 km away from the epicenter, and JMA = 3 at another one located 35 km away. The distance between stations caused a delay in the activation of the MASLIS, which detected the earthquake 15 s after the origin time (AT-OT in Table 4). The first warning message reached the public 11 seconds later (TT-AT in Table 4). A total of 26 s had passed since OT and the P-waves (black dotted circle in Fig. 10) were about to arrive in San Jose. The S-waves had traveled 92 km from the hypocenter and were already shaking Liberia and Canas cities. The red circle corresponds to the late alert zone (McBride et al., 2020). This is the area where any notification from an impending earthquake will arrive after the damaging S-waves. There were a total of 28 s left before the S-wave arrived in San Jose.

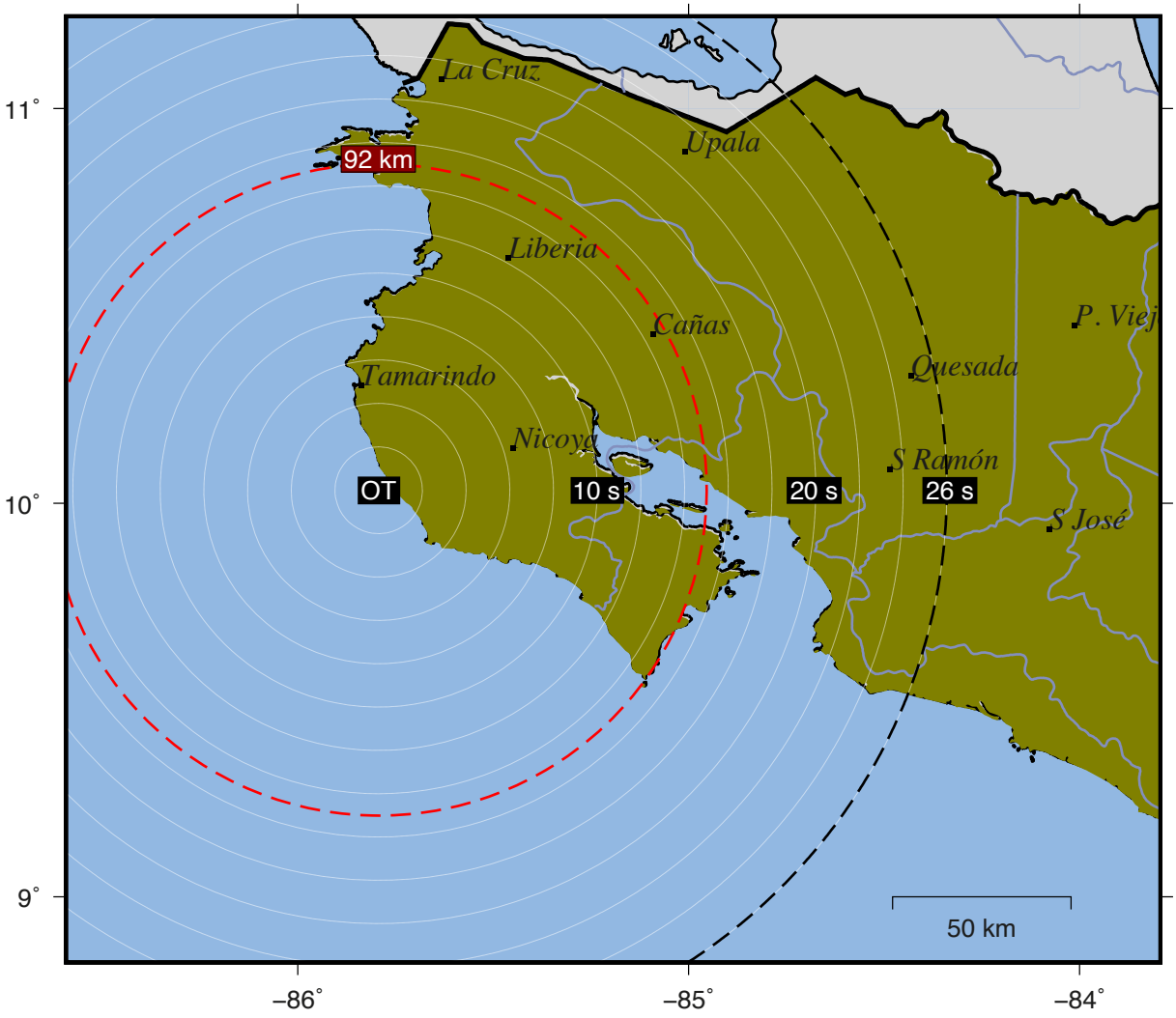

Figure 10. Wave propagation for event number 1 in Tables 3 and 4. The black dotted circle corresponds to the approximate location of the P-wave front at the time in seconds when the first message was received by the public. The red dotted circle shows the distance traveled by the S-wave from the source. Thin white lines represent the propagation times of P-waves in 2-second intervals. In this case, there were 28 seconds of warning time before the S-waves arrived in San Jose.

That event was very close to the epicenter of the September 5th, 2012, M7.6 Nicoya earthquake (Yue et al., 2013; Fig. 2). The Nicoya earthquake was the largest event to hit Costa Rica in the last 20 years. The epicenter was located some 12 km off the northern Pacific coast. The intensity reached JMA = 6– at the closest station. In San Jose,

the mean intensity was JMA = 4. Much of the damage was limited to the epicentral region due to the strong ground motion. Nevertheless, soil amplification effects caused some damage in the western GAM as observed by Schmidt et al. (2014).

5.2 Southern Pacific Region

On July 21st, 2021, an M6.7 earthquake occurred offshore the Panama-Costa Rica border. It was the largest earthquake recorded by the MASLIS in the past five years. Due to the magnitude and distant epicenter location (308 km from San Jose), initial records showed long-period waves with emergent rather than impulsive P-wave amplitudes. This resulted in a delayed activation of the MASLIS due to the increased time required to reach JMA = 2. The trigger threshold in 2021 was JMA = 2 at two sites. The first alert was issued 46 seconds after OT (Table 4) when the P-waves were close to arriving in Turrialba and Limon cities (Fig. 11a). The S-waves had traveled 162 km from the source. There were 41 seconds before the S-waves arrived in San Jose (Table 4).

Two years later, on April 4th, 2023, an M6.4 earthquake occurred east of the M6.7 earthquake as shown in Fig. 11b. It was located 326 km away from San Jose. This time, the MASLIS trigger threshold had been changed from JMA = 2 to JMA = 1. The first warning message was sent 35 seconds after OT when the P-waves were about to arrive in San Isidro city. In terms of time, the system responded 10 seconds faster compared to the 2021 event. The S-wave front was 132 km from the epicenter and it would arrive in San Jose in 51 seconds. The late alert zone area decreased by an estimated 33%.

The SPR is a very active zone as shown in Fig. 1. Significant subduction events happened in 1904, 1941, and 1983, suggesting a recurrence period of approximately 40 years (Adamek et al., 1987). The next two events are located inland near the epicenter of the 1983 earthquake (Fig. 12), and they can give us a rough estimation of the potential warning times for a future stronger event.

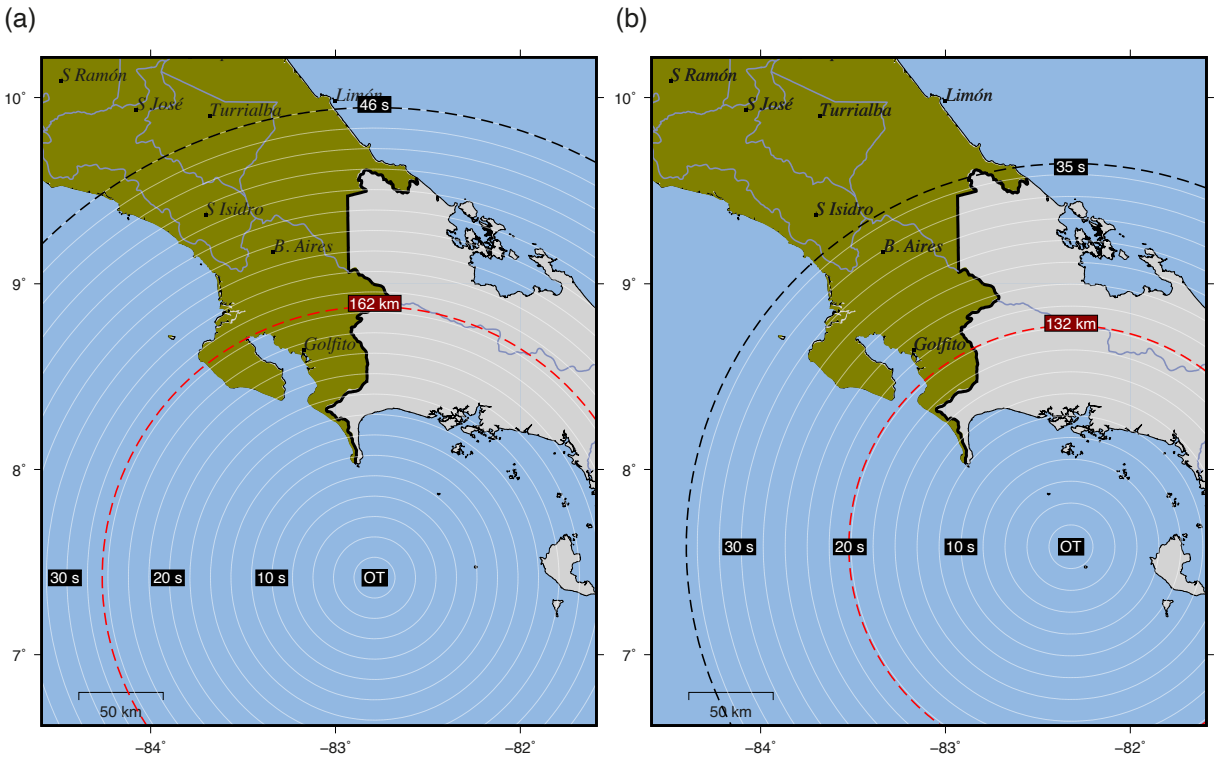

Figure 11. In (a) the 2021-07-21-M6.7 earthquake triggered by using JMA = 2 threshold. In (b) the 2023-04-04-M6.4 event triggered by using JMA = 1 threshold. The black dotted circle corresponds to the approximate location of the P-wave front at the time in seconds when the first message was received by the public. The red dotted circle shows the distance traveled by the S-wave from the source. Thin white lines represent the propagation times of P-waves in 2-second intervals.

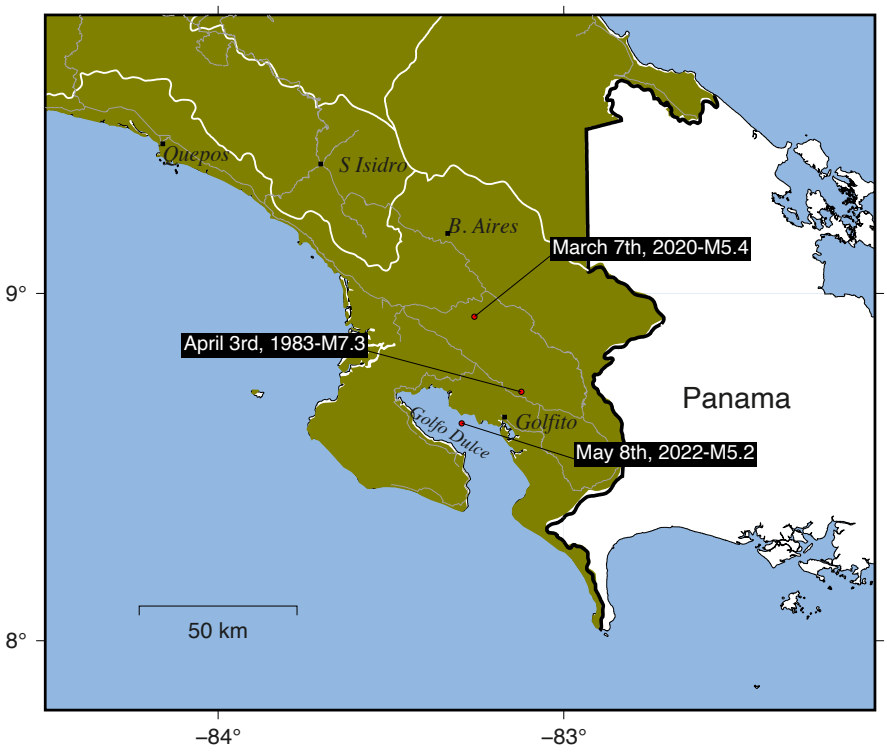

Figure 12. Epicenter of the 1983 Ms 7.3 Golfito earthquake and two other recent events that were recorded by the MASLIS in 2020 and 2022. The white lines correspond to administrative divisions, and gray lines represent major roads.

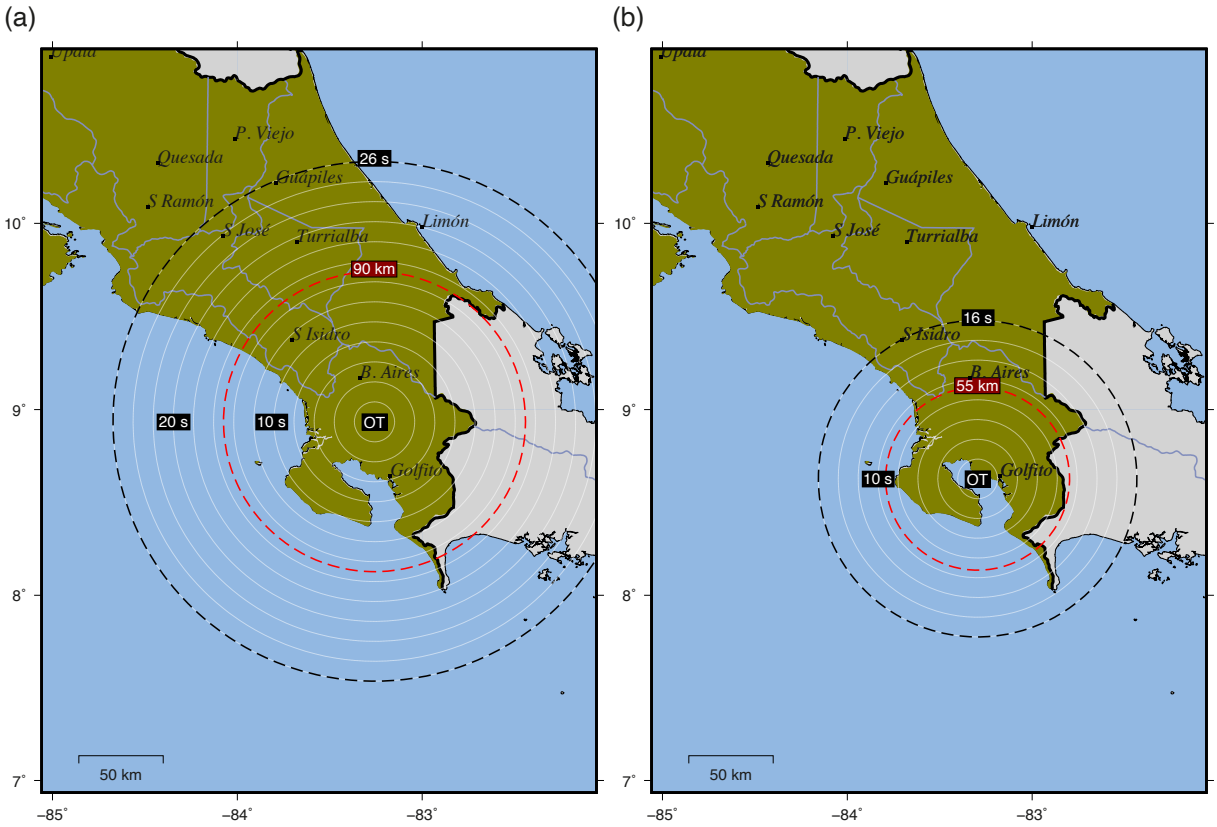

Figure 13. Travel times for the (a) M5.4 March 7th, 2020 event and (b) M5.2 May 08th, 2022 event. The black dotted circle corresponds to the approximate location of the P-wave front when the first message was received by the public. The red dotted circle shows the distance traveled by the S-wave from the source. Thin white lines represent the propagation times of P-waves in 2-second intervals.

On March 7th, 2020, an M5.4 earthquake at 50 km depth struck the southern region (Fig. 13a). Because this was a relatively deep-focus event, by the time the seismic waves reached the surface, they triggered several stations at once, even though they were located some 25 km apart from each other. The MASLIS sent the first message 26 s after the earthquake. By that time, the P-waves had already reached San Jose while the S-waves had traveled 90 km from the source. There was a 15 s warning time before the S-waves arrived in San Jose.

Another event happened on May 8, 2022, with a magnitude of 5.2 (Fig. 13b). Its epicenter was located inside Golfo Dulce, a region surrounded by seven stations. The depth of the earthquake was 14 km. The MASLIS issued the first message 16 seconds after OT when the S-waves had traveled 55 km from the source (Table 4). There was a 32-second warning time before the S-waves arrived in San Jose.

5.3 Central Pacific Region

On August 24th, 2020, an M6.0 earthquake struck 8 km off the coast of Jaco city, causing buildings to sway in San Jose (Fig. 14). The estimated depth was 22.7 km. The MASLIS was triggered 11 seconds after OT (Table 4), but it took 13 more seconds for the first message to reach the public. The S-waves had already arrived in San Jose. The delay was caused because one of the two stations located in Jaco city was offline at the time of the earthquake. The next closest station was located 30 kilometers away. This situation resembles the event studied in the northern Pacific, where the distance between activated stations exceeded 30 km. The seismic intensity was JMA = 5 in Jaco city.

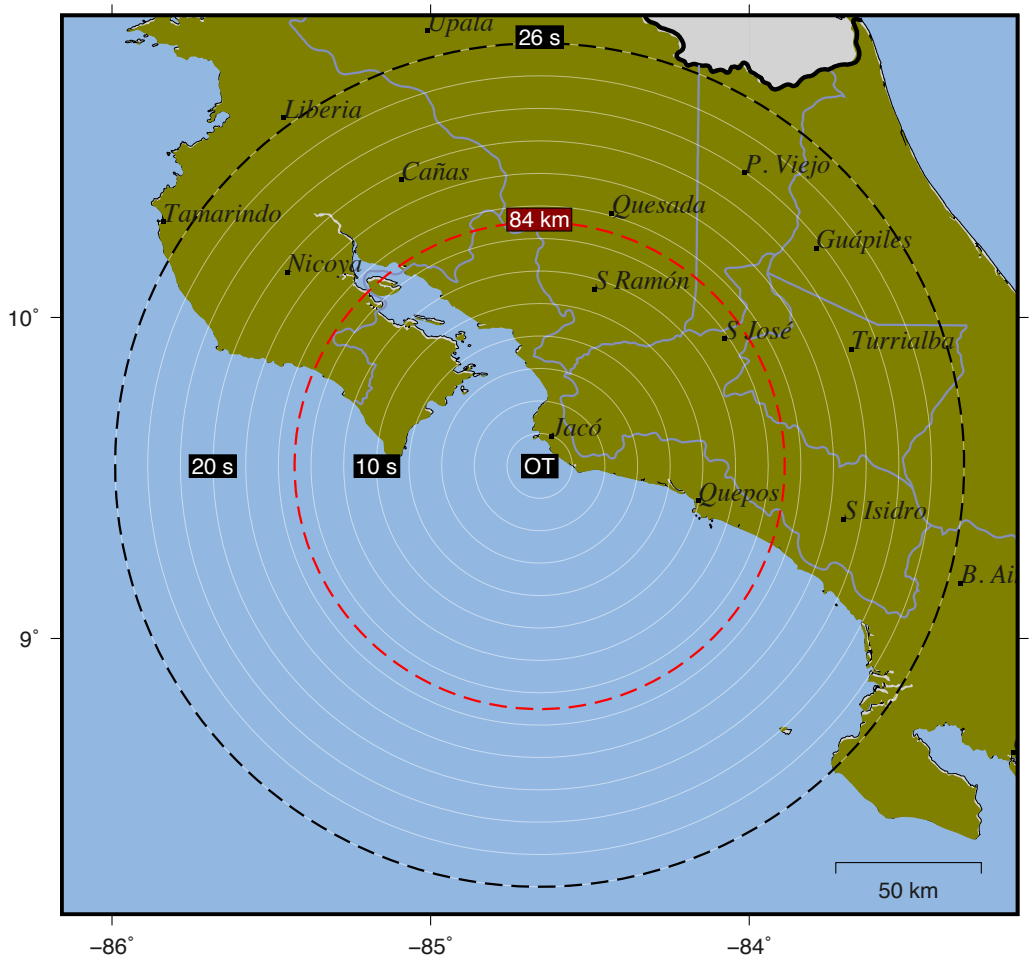

Figure 14. Propagation time for the August 24th, 2020, M6.0 earthquake in front of Jaco city. The black dotted circle corresponds to the approximate location of the P-wave front when the first message was received by the public. The red dotted circle shows the distance traveled by the S-wave from the source. Thin white lines represent the propagation times of P-waves in 2-second intervals.

5.4 Inland Central Region

The MASLIS has recorded 61 earthquakes whithin the ICR (Table 2; Fig. 8). Most of the events are related to faults in the area. A smaller group happened deeper than 50 km and could be associated to internal deformation of the subducted plate. Receiving warning messages before the strong S-waves reach San Jose is challenging due to the close proximity of seismic sources to the capital.

On February 18th, 2023 the MASLIS recorded an M5.3 event very close to the epicenter of the M6.2, 2009 earthquake (Fig. 3; Fig. 6; Fig. 15a). It was a shallow event located 32 km away from San Jose and at 6.5 km depth. The MASLIS detected the earthquake in 6 s (Table 4). It processed the information in the following 6 s and 2 s later the information reached the public. However, at that time, the S-waves had reached San Jose after traveling approximately 45 km from the epicenter.

The same year, on July 12th, the MASLIS also recorded another shallow M4.0 earthquake near the epicenter of the M6.0, 1990 earthquake (Fig. 3; Fig. 7; Fig. 15b). Even though the earthquake was detected within 7 seconds (Table 4), it took nearly twice as long to process the data. This particular event could be consider an outlier because AT-OT is generally larger than CT-AT.

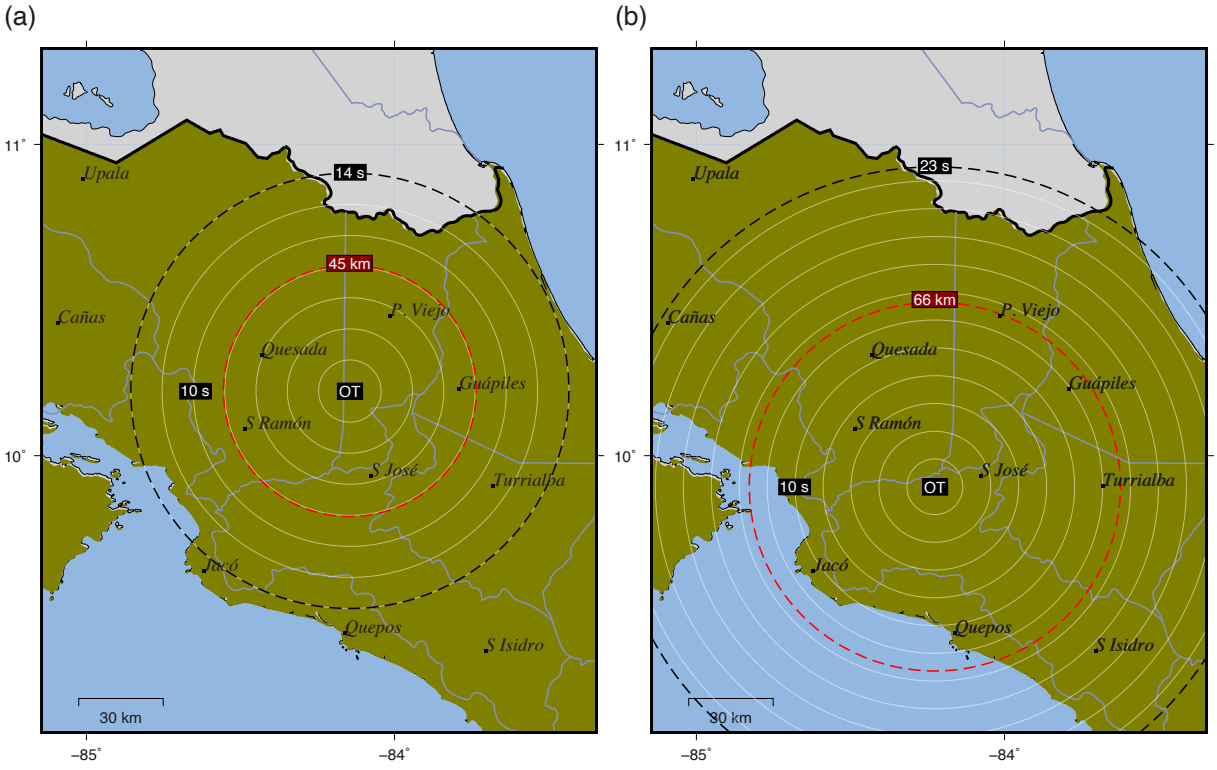

Figure 15. In (a) epicenter of the February 8th, 2023 M5.3 earthquake. In (b) the July 12th, 2023 M4.0 earthquake near the city of San Jose. The black dotted circle corresponds to the approximate location of the P-wave front at the time when the first message was received by the public. The red dotted circle shows the distance traveled by the S-wave from the source. Thin white lines represent the propagation times of P-waves in 2-second intervals.

6. Results and Discussion

From the analysis of the different seismogenic zones, we can see that the current version of the MASLIS fails to send any warning messages to San Jose when the earthquakes are located in the ICR or CPR. The reason is that the shortest TT-OT (Table 4) ranges from 14 s to 16 s for a corresponding 45 to 55 km S-wave distance traveled from the hypocenter. The nearby local faults and central subduction zone are within that range.

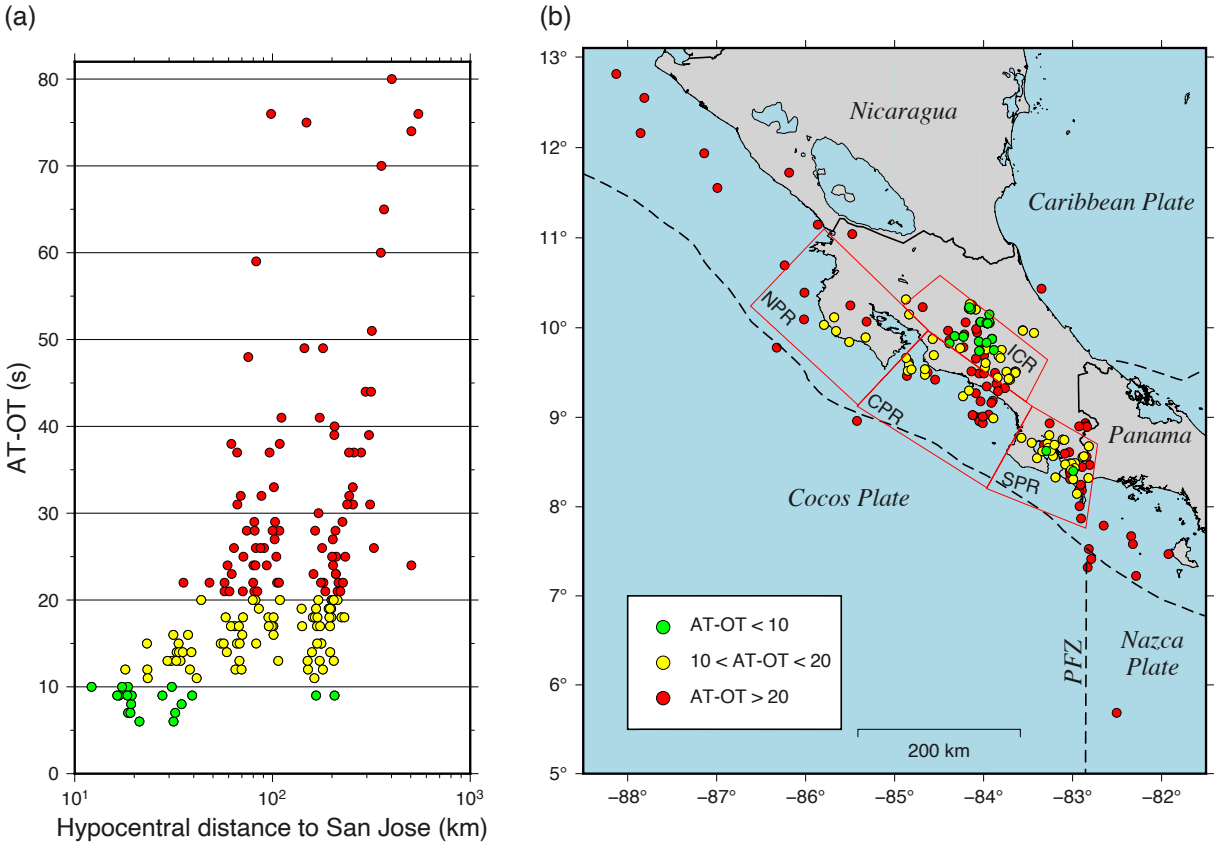

Figure 16. In (a) AT-OT difference versus hypocentral distance from San Jose for all events in this study. In (b) the location of the same events as a function of AT-OT. In green, the events with AT-OT less than 10 s, in yellow the events with AT-OT less than 20 s, and in red the rest.

The MASLIS's activation time varies significantly depending on the earthquake's location and depth. Figure 16a shows AT-OT as a function of hypocentral distance to San Jose for all events in this study, while Fig. 16b displays their location on the map. The events with detection times below 10 s are highlighted in green. They make up just 10% of the total and are mostly located close to the GAM. Only two of them were located in the southern Pacific region. It is clear from the figure that earthquakes outside the strong-motion network will consistently experience delayed detection times.

To further evaluate the system's performance, we plotted the processing time, CT-AT, and posting time, TT-CT, as a function of the last one hundred recorded events (yellow squares in Fig. 17). The last one hundred events were

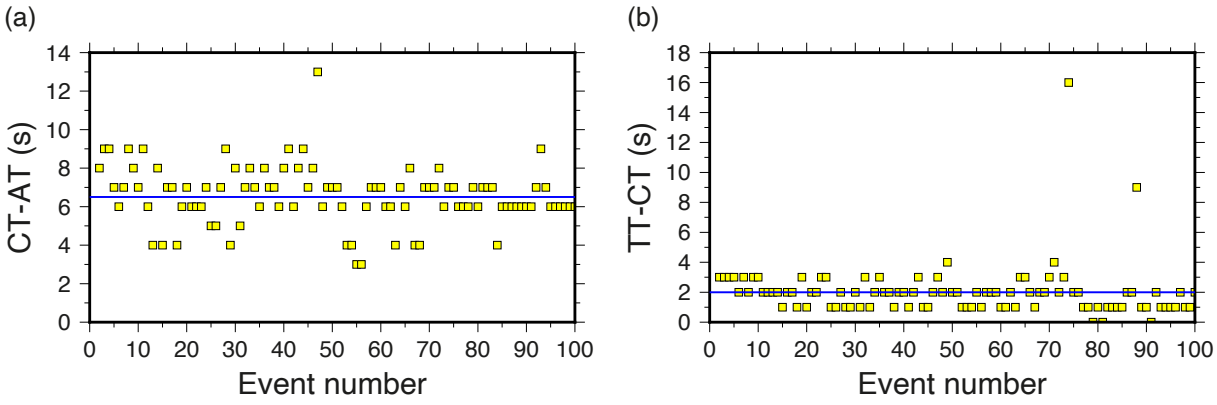

Figure 17. (a) Processing (CT-AT) and (b) posting (TT-CT) times as a function of earthquake number for the last one-hundred events (yellow squares) recorded by the MASLIS. The blue line corresponds to the average.

the ones triggered when the threshold was changed to JMA = 1. Figure 17a shows the result for CT-AT as a function of event number. On average, the system takes approximately 6.5 s (blue line) in order to process all information after an earthquake has been detected. The standard deviation is 1.5 s. The shortest processing time is 3 s, while the longest is 13 s. The latter correspond to the event from July 12th, 2023 that was shown above (Fig. 15b).

Figure 17b shows the time it takes for the messages to be posted on Telegram. This time was extracted from the final posting time shown on Telegram. Both the average and the median are 2 s (blue line). There are two outliers of 16 seconds and 9 seconds, which are probably related to communications problems. No analysis was performed on X because the social network only showed the hour and minute of the post, not the seconds.

Figure 18 shows the network's latency. Currently, 55% of the network experienced latency below 1 s, 31% had higher latency, and 14% were offline. Low latency is associated with new strong-motion instruments that have been purchased by the LISUCR in recent years and are expected to replace the old ones in the future. Furthermore, the 31% also corresponds to instruments that use a different data format. Therefore, some of the delay can be attributed to the process of converting the data from its original format to the standard one used throughout the network.

The percentage of offline units is never constant and it is a challenging task because the MASLIS is not part of any first-response or emergency system. The instruments are located in places with variable speed rates and bandwidth. A given station can be offline for several hours or days due to local area problems. This is what affected the early detection of the M6.0 that struck in front of Jaco city on August 24th, 2020 (Tables 3 and 4), as mentioned earlier.

The MASLIS calculates the source parameters as complementary information only. Figure 18 shows the difference in values between the original source parameter calculated by the MASLIS and the updated final values. In every

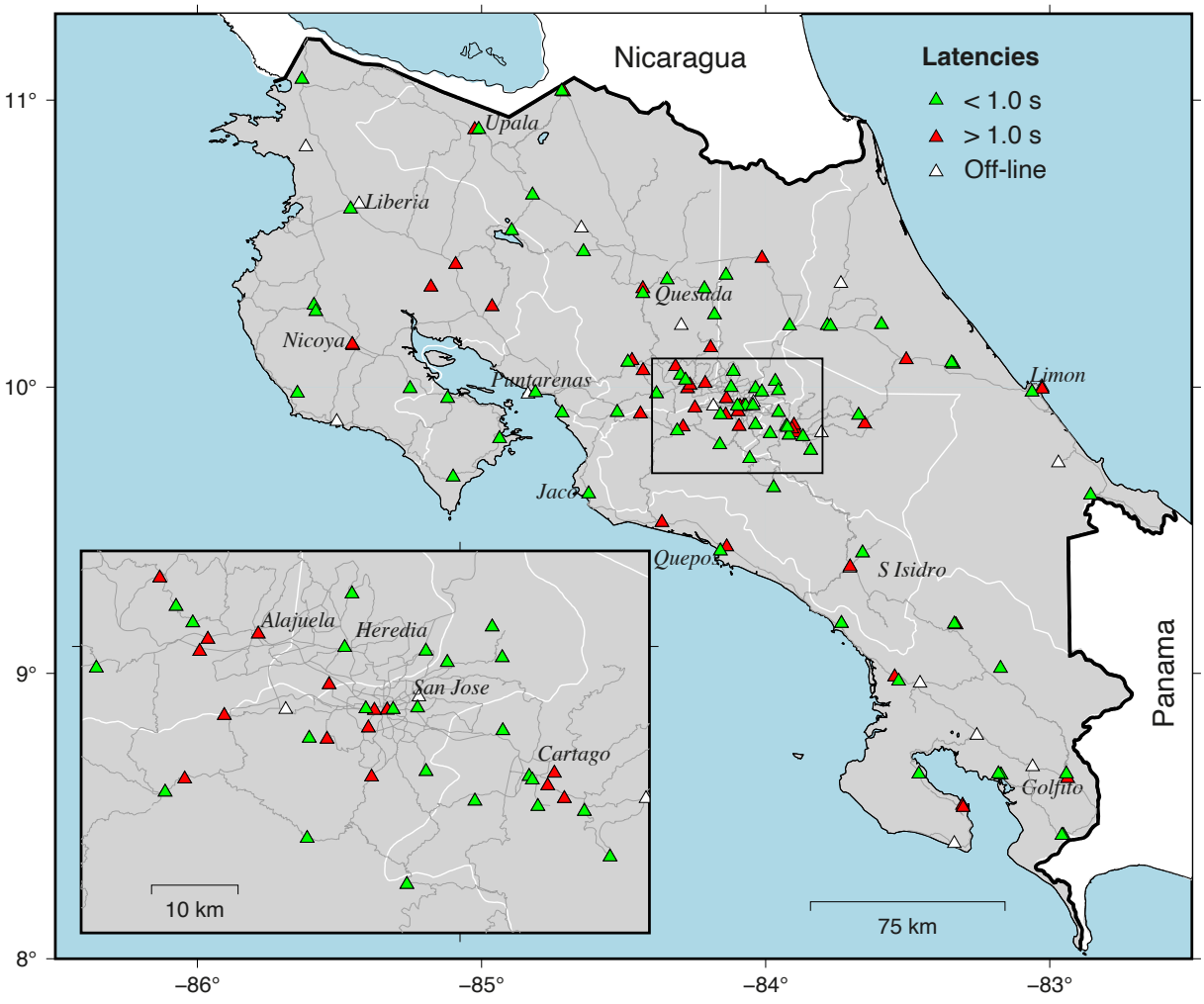

Figure 18. Latencies in the LISUCR's strong-motion network. Green triangles show the stations where latency is less or equal to 1 s, red triangles show stations with higher values. White triangles show stations offline at the time of this writing. The figure does not include the stations from OVSICORI.

instance, the correlation coefficient R^2 exceeds 0.8. The black line shows the trend line. The red dot is an outlier that corresponds to a magnitude 6.5 event that happened on July 19, 2023, offshore northern Nicaragua (Fig. 8). The system mislocated the epicenter closer to Costa Rica as shown in Figs. 19a and 19b. The MASLIS estimated its magnitude at 5.7 (Fig. 19c). Another important event highlighted in yellow corresponds to a magnitude 5.9 earthquake that happened on August 3rd, 2023, along the PFZ. The epicenter was incorrectly placed by MASLIS near 7.5 latitude instead of 5.5 (Figs. 19a and 19b). That was a 2-degree difference. In addition to that, the MASLIS also estimated its magnitude at 5.0 (Fig. 19c). In general, the system cannot reliably estimate the magnitude for distant events (this includes deep-focus earthquakes) because the displacement spectra will predominantly consist of P-waves during the calculation process.

The average error, E, is also shown in the figure. Differences in longitude and latitude estimation are within 0.1 degrees. The error is greatly influenced by the mislocations of the M6.5 and M5.9 events. On average, the depth fluctuates within a range of 5 km, while the magnitude varies by 0.2 units. However, if we remove the outliers, the error decreases to 0.03 degrees for longitude and latitude, and 0.13 units for the magnitude. The accuracy of source parameters seems to increase when earthquakes occur within the boundaries of the network.

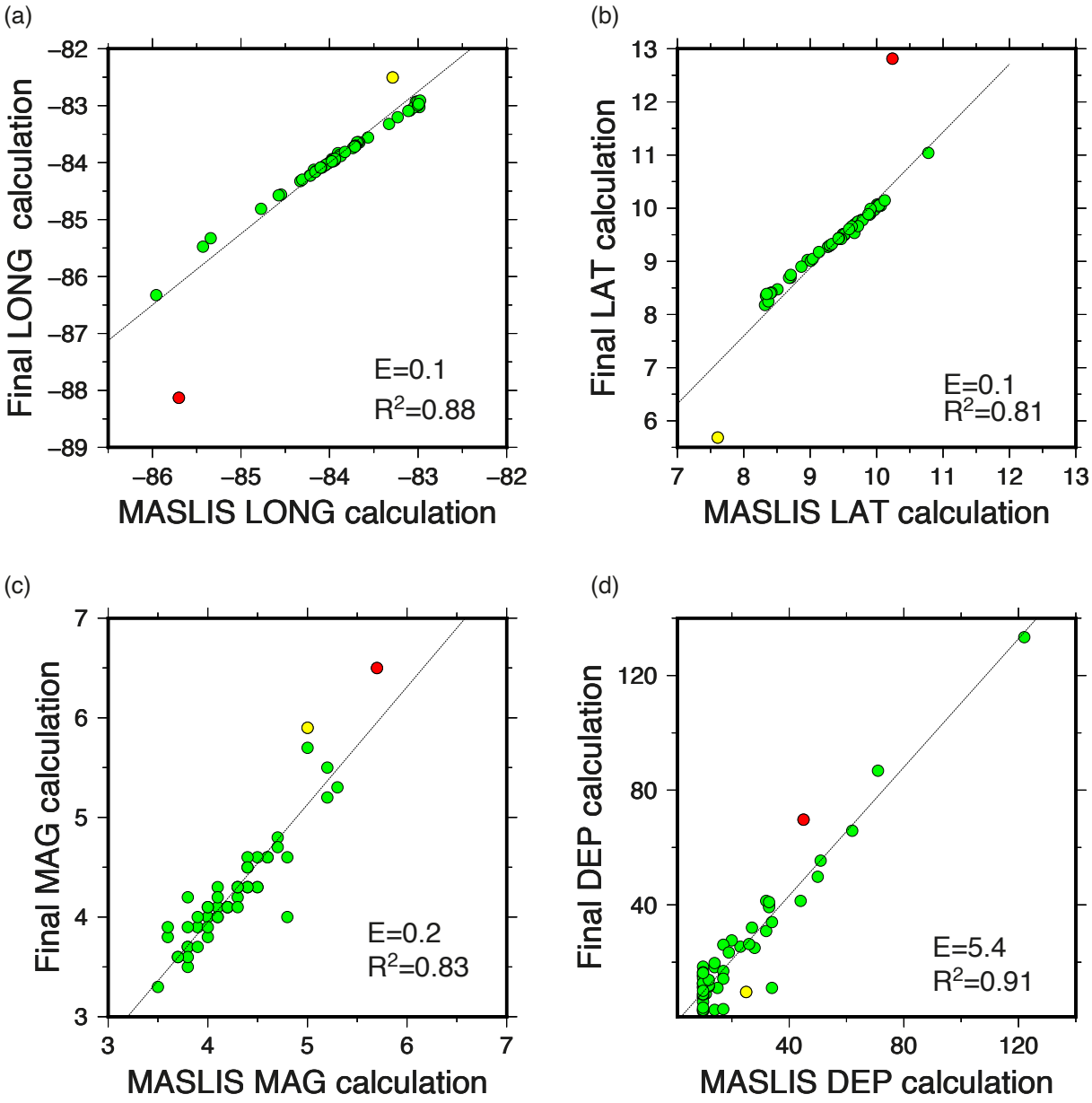

Figure 19. Comparison between the source parameters (LONGitude, LATitude, MAGnitude, and DEPth) between the MASLIS estimation and the final revised calculation. The correlation coefficiet, R^2, is shown in each plot as well as the average error, E.

7. Conclusions

1) The MASLIS reads and processes strong motion data in order to calculate the PGA, and JMA intensity. When an earthquake is detected, a warning message is issued that contains information about the strengh of the shaking.
2) The processing time after an event has been detected is 6.5 s on average. There is another 2 s delay before the message gets to the recipients. Information gets to the public through social networks such as X and Telegram.
3) In the best-case scenario, a shallow hypocenter surrounded by many stations, the late alert zone has a radius of approximately 50 km. This means that, for the specific case of San Jose, only earthquakes located in the NPR and SPR (Fig. 16) of Costa Rica will be processed quickly enough to issue a warning time before the S-waves arrive in the capital.
4) The MASLIS calculates the source parameters as complementary information. They are not used to activate the system, nor are they used to carry out any ground motion prediction at target locations to generate custom alerts. This computation is conducted in a parallel module, so it does not interfere with the rest of the processing steps shown in Table 4.
5) Adding new stations to the strong-motion network could improve the performance of MASLIS. They are required in the country's northern, southern, and eastern regions. In those areas, the stations are located more than 30 km apart.
6) The system can benefit from the acquisition of new technology specifically designed for early warning. Current strong-motion instruments use standard data compression and sample rates (typically 200 Hz), which increase the delays in data transmission.
7) Even though the MASLIS is not fully an EEWS, the information on the shaking intensity it provides could be valuable to emergency response authorities.

References

Adamek, S., F. Tajima and D. A. Wiens (1987). Seismic rupture associated with subduction of the Cocos Ridge, Tectonics, 6, 6, 757-774. doi:10.1029/tc006i006p00757.

Allen, R. M. and D. Melgar (2019). Earthquake Early Warning: Advances, Scientific Challenges, and Societal Needs, Annu. Rev. Earth Pl. Sci.,47, 361-88. doi:10.1146/annurev-earth-053018-060457.

Alonso-Henar, J., W. Montero, J. Martinez-Diaz, J. Alvarez-Gómez et al. (2013). The Aguacaliente Fault, source of the Cartago 1910 destructive earthquake (Costa Rica), Terra Nova, 25, 368-373. doi:10.1111/ter.12045.

Andrews, D. J. (1986). Objective determination of source parameters and similarity of earthquakes of different size, Geophys. Monogr. Ser., 37, 6, 259-267.

Bilek, S. and C. Lithgow-Bertelloni (2005). Stress change in the Costa Rica subduction zone due to the 1999 Mw = 6.9 Quepos earthquake, Earth Planet. Sci. Lett., 230, 97-112, doi:10.1016/j.epsl.2004.11.020.

Bilek, S. L., C. E. Elliott and C. L. Bertelloni (2009). Triggered seismicity associated with the 1990 Nicoya, Costa Rica, Mw = 7.0 earthquake, Geochem. Geophys. Geosys., 10, Q04S13, doi:10.1029/2008GC002317.

Bird, P. (2003). An updated digital model of plate boundaries, Geochem. Geophys. Geosys., 4, 3, doi:10.1029/2001GC000252.

Brooks, B. A., M. Protti, T. Ericksen, J. Bunn et al. (2021). Robust earthquake early warning at a fraction of the cost: ASTUTI Costa Rica, AGU Advances, 2, e2021AV000407, doi:10.1029/2021AV000407.

Brune, J. N. (1970). Tectonic stress and the spectra of seismic shear waves from earthquakes, J. Geophys. Res., 75, 4997-5009.

Burkett, E. R., D. D. Given and L. M. Jones (2014). ShakeAlert: an earthquake early warning system for the United States West Coast, U.S. Geological Survey Fact Sheet, 2014-3083, Fact Sheet: 4. doi:10.3133/fs20143083.

Chung, A. I., M. A. Meier, J. Andrews, M. Böse et al. (2020). ShakeAlert earthquake early warning system performance during the 2019 Ridgecrest earthquake sequence, Bull. Seismol. Soc. Am., 110, 4, 1904-1923.

Clinton, J., A. Zollo, A. Marmureanu, C. Zulfikar et al. (2016). State-of-the art and future of earthquake early warning in the European region, Bull. Earthq. Eng., 14, doi:10.1007/s10518-016-9922-7.

Espinosa-Aranda, J., A. Jiménez, G. Ibarrola, F. Alcantar, et al. (1995) Mexico City Seismic Alert System, Seismol. Res. Lett., 66, 42-53.

Fujinawa, Y. and Y. Noda (2013). Japan's Earthquake Early Warning System on 11 March 2011: Performance, Shortcomings, and Changes, Earthq. Spectra, 29, 1, 341-368, doi:10.1193/1.4000127.

Goess, S., A. Velasco, S. Schwartz and T. Lay (1993). The April 22, 1991, Valle de la Estrella, Costa Rica (Mw = 7,7) earthquake and its tectonic implications: A broadband study, J. Geophys. Res., 98, 8127-8142.

Goldstein, P. and A. Snoke (2005). SAC Availability for the IRIS Community, Incorporated Institutions for Seismology Data Management Center Electronic Newsletter.

Hanks, T. C. and H. Kanamori (1979). A Moment Magnitude Scale, J. Geophys. Res., 84, 2348-2350, doi:10.1029/JB084iB05p02348.

Hidalgo-Leiva, D., L. Linkimer, I. Arroyo, M. Arroyo-Solórzano et al. (2022). The 2022 Seismic Hazard Model for Costa Rica, Bull. Seismol. Soc. Am., 113, 1, 23-40. doi:10.1785/0120220119.

Hoshiba, M., O. Kamigaichi, M. Saito, S. Tsukada et al. (2008). Earthquake Early Warning Starts Nationwide in Japan. Eos Trans., AGU, 89, 73-74, doi:10.1029/2008EO080001.

Hoshiba, M. and K. Iwakiri (2011). Initial 30 seconds of the 2011 off the Pacific coast of Tohoku Earthquake (Mw 9.0)-amplitude and τc for magnitude estimation for Earthquake Early Warning, Earth Planets Space, 63, 553-557.

Husen, S., R. Quintero, E. Kissling and B. Hacker (2003). Subduction zone structure and magmatic processes beneath Costa Rica constrained by local earthquake tomography and petrological modelling, Geophys. J. Int., 155, 11-32, doi:10.1046/j.1365-246X.2003.01984.x.

Kodera, Y., N. Hayashimoto, K. Tamaribuchi, K. Noguchi et al. (2021). Developments of the Nationwide Earthquake Early Warning System in Japan After the 2011 M w 9.0 Tohoku-Oki Earthquake, Front. Earth Sci., 9,726045, doi:10.3389/feart.2021.726045.

Lomax, A., J. Virieux, P. Volant and C. Berge-Thierry. Probabilistic Earthquake Location in 3D and Layered Models. In: Thurber C.H., Rabinowitz N. (eds) (2000). Advances in Seismic Event Location, Modern Approaches in Geophysics, 18, Springer, Dordrecht, doi:10.1007/978-94-015-9536-0_5.

Lücke, O. H. and I. G. Arroyo (2015). Density structure and geometry of the Costa Rican subduction zone from 3-D gravity modeling and local earthquake data, Solid Earth, 6, 4, 1169-1183, doi:10.5194/se-6-1169-2015.

Lux, A. I., D. Smith, M. Böse, J. J. McGuire et al. (2024). Status and Performance of the ShakeAlert Earthquake Early Warning System: 2019-2023, Bull. Seismol. Soc. Am., doi:10.1785/0120230259.

McBride, S. K., A. Bostrom, J. Sutton, R. M. de Groot et al. (2020). Developing post-alert messaging for ShakeAlert, the earthquake early warning system for the West Coast of the United States of America. Int. J. Disast. Risk Re., 50, 101713.

Morrel, K. D., D. M. Fisher and T. W. Gardner (2008). Inner forearc response to subduction of the Panama Fracture Zone, southern Central America, Earth Planet Sci. Lett., 265, 1-2, 82-95.

Moya, A. (2017). Sistema de monitoreo acelerográfico del Laboratorio de Ingeniería Sísmica, Revista Ingeniería, 28, 96, doi:10.15517/ri.v28i1.30874.

Moya, A. (2019). Monitoreo Acelerográfico Secundario del Laboratorio de Ingeniería Sísmica (MAS-LIS) y su potencial para usarlo como un sistema de alerta temprana para terremotos, Ingeniería, 29, 1, 1-20.

Moya-Fernández, A., L. A. Pinzón, V. Schmidt-Díaz, D. A. Hidalgo-Leiva et al. (2020). A Strong-Motion Database of Costa Rica: 20 Yr of Digital Records, Seismol. Res. Lett., 91, 6, 3407-3416, doi:10.1785/0220200036.

Pacheco, J. F., R. Quintero, F. Vega, J. Segura et al. (2006). The Mw 6.4 Damas, Costa Rica, Earthquake of 20 November 2004: Aftershocks and Slip Distribution, Bull. Seismol. Soc. Am., 96, 1-12.

Peng, C., P. Jiang, Q. Ma, P. Wu et al. (2021). Performance evaluation of an earthquake early warning system in the 2019-2020 M6.0 Changning, Sichuan, China, seismic sequence, Front. Earth Sci., 9, 1-13, doi:10.3389/feart.2021.699941.

Porras, J., F. Massin, M. Arroyo-Solórzano, I. Arroyo et al. (2021). Preliminary Results of an Earthquake Early Warning System in Costa Rica, Front. Earth Sci., 9, 700843, doi:10.3389/feart.2021.700843.

Protti, M., K. McNally, J. Pacheco, V. González et al. (1995). The March 25, 1990 (Mw = 7.0, ML = 6.8), earthquake at the entrance of the Nicoya Gulf, Costa Rica: Its prior activity, foreshocks, aftershocks, and triggered seismicity, J. Geophys. Res., 100, B10, 20, 345-20, 358, doi:10.1029/94JB03099.

Protti, M. (2001). Significance of an earthquake early warning system for vulnerable essential facilities: the example of a potential implementation in Costa Rica. ISDR informs: a magazine for Latin America and the Caribbean, 3:21-24.

Quesada-Román, A. and G. Barrantes-Castillo (2016). Procesos de ladera cosísmicos del terremoto de Cinchona (Costa Rica) del 8 de enero de 2009 (Ms = 6,2). Cuadernos de Geografía: Revista Colombiana de Geografía, 25,

1, 217-232. [fecha de Consulta 18 de Junio de 2024]. ISSN: 0121-215X. Recuperado de: https://www.redalyc.org/articulo.oa?id=281843790015.

Satriano, C., L. Elia, C. Martino, M. Lancieri et al. (2011). PRESTo, the earthquake early warning system for Southern Italy: Concepts, capabilities and future perspectives, Soil Dyn. Earthq. Eng., 31, 2, 137-153, ISSN 0267-7261, doi:10.1016/j.soildyn.2010.06.008.

Schmidt, V., D. Hidalgo, A. L. Acuña, A. Moya et al. (2014). Aceleraciones del terremoto de Sámara del 05 de setiembre del 2012, Revista En Torno a la Prevención, 12, 38-47.

Shabestari, K. and F. Yamazaki (2001). A Proposal of Instrumental Seismic Intensity Scale Compatible with MMI Evaluated from Three-Component Acceleration, Earthq. Spectra, 17, 4, 711-723.

Suárez, G., M. Pardo, J. Domínguez, L. Ponce, et al. (1995). The Limón, Costa Rica earthquake of April 22, 1991 (Mw = 7.7): Evidence of back-arc thrusting and collisional tectonics in a subduction environment, Tectonics, 14, 518-530.

Suárez, G. (2022). The Seismic Early Warning System of Mexico (SASMEX): A Retrospective View and Future Challenges, Front. Earth Sci., 10, 827236, doi:10.3389/feart.2022.827236.

Tajima, F. and M. Kikuchi (1995). Tectonic implications of the seismic ruptures associated with the 1983 and 1991 Costa Rica earthquakes in Geologic and Tectonic Development of the Caribbean Plate Boundary in Southern Central America, Boulder, Colorado, The Geological Society of America Special Paper, 295, 327-340.

Wald, D. (2020). Practical limitations of earthquake early warning, Earthq. Spectra, 36, 1412-1447, doi:10.1177/8755293020911388.

Wessel, P., W. H. F. Smith, R. Scharroo, J. F. Luis et al. (2013). Generic Mapping Tools: Improved version released, Eos Trans, AGU, 94, 45, 409-410, doi:10.1002/2013EO450001.

Wu, Y. M., H. Mittal, D. Y. Chen, T. Y. Hsu et al. (2021). Earthquake Early Warning Systems in Taiwan: Current Status, J. Geol. Soc. India, 97, 1525-1532, doi:10.1007/s12594-021-1909-6.

Ye, L., L. Thorne and H. Kanamori (2013). Large earthquake rupture process variations on the Middle America megathrust, Earth Planet. Sci. Lett., 381, 147-155.

Yue, H., T. Lay, S. Y. Schwartz, L. Rivera et al. (2013). The 5 September 2012 Costa Rica Mw 7.6 earthquake rupture process from joint inversion of high-rate GPS, strong-motion, and teleseismic P wave data and its relationship to adjacent plate boundary interface properties, J. Geophys. Res., 118, 5453-5466, doi:10.1002/jgrb.50379.

Zhang, M., X. Quao, B. C. Seyler, B. Di et al. (2021). Brief communication: Effective earthquake early warning systems: Appropriate messaging and public awareness roles, Nat. Hazard Earth Sys., 21, c.3243, doi:10.5194/nhess-21-3243-2021.

***CORRESPONDING AUTHOR: Aaron MOYA**,
Laboratorio de Ingeniería Sísmica, Universidad de Costa Rica
e-mail: cesar.moya@ucr.ac.cr